Title

Mechanisms of mitotic spindle function in Saccharomyces cerevisiae

Permalink

https://escholarship.org/uc/item/529955j4

Author

Ibarlucea Benitez, Itziar

Publication Date

2017

Peer reviewed|Thesis/dissertation

Mechanisms of mitotic spindle function in *Saccharomyces cerevisiae*

By

Itziar Ibarlucea Benítez

A dissertation submitted in partial satisfaction of the

requirements for the degree of

Doctor of Philosophy

in

Biophysics

in the

Graduate Division

of the

University of California, Berkeley

Committee in charge:

Professor Georjana Barnes, Co-chair
Professor David G. Drubin, Co-chair
Professor Eva Nogales
Professor Rebecca Heald
Professor Douglas Koshland

Spring 2017

Mechanisms of mitotic spindle function in *Saccharomyces cerevisiae*

Abstract

Mechanisms of mitotic spindle function in *Saccharomyces cerevisiae*

by

Itziar Ibarlucea Benítez

Doctor of Philosophy in Biophysics

University of California, Berkeley

Professor Georjana Barnes, Co-chair
Professor David G. Drubin, Co-chair

Cell division is an essential process for multicellular organisms. The fundamental goal of mitosis is to duplicate and segregate the genetic material of one cell, to ultimately generate two cells genetically identical to each other and to the parent cell. The mitotic spindle is a microtubule-based structure that attaches to, and segregates replicated chromosomes to the two daughter cells. To accomplish such a crucial, yet intricate task, the mitotic spindle must be correctly assembled, positioned, and disassembled. Historically, research has mostly focused on addressing the first problem. However, recent studies have highlighted the importance of proper spindle positioning and disassembly. In this dissertation we attempt to address these last two problems. We focused on understanding how the activities of a group of microtubule-associated proteins are coordinated to regulate microtubule function during spindle positioning and disassembly, to finally ensure successful cell division.

The work presented in Chapters 2 and 3 of this dissertation attempts to shed light on the process of spindle disassembly. The Aurora B protein kinase, or Ipl1 in budding yeast, is one of the main regulators of spindle disassembly. Once chromosome segregation is completed, and just before the onset of spindle disassembly, the Ipl1/Aurora B kinase concentrates at the spindle midzone, the region of spindle breakage. However, we do not fully understand how it is targeted to the midzone, or its precise role there. Chapter 2 addresses these two questions. Combining live cell microscopy with yeast genetics and biochemistry we identified a kinesin-5 (Kip1) as the main kinesin responsible for the midzone localization of Ipl1/Aurora B. Kip1 alone is sufficient to recruit Ipl1/Aurora B to microtubules, and it is able to transport Ipl1/Aurora B to the microtubule end. We also found that cells rely on cytokinesis to physically break the spindle if the Ipl1/Aurora B kinase cannot concentrate at the midzone. Once at the midzone, we know that Ipl1/Aurora B phosphorylates targets to destabilize the spindle and allow its breakage. She1 is a microtubule-associated protein that is activated during late anaphase by Ipl1/Aurora B-mediated phosphorylation. However, we do not understand its precise role during spindle disassembly. Chapter 3 investigates this question, and addresses whether She1 promotes spindle disassembly by directly destabilizing spindle microtubules.

The mitotic spindle needs to be positioned perpendicular to the division plane for proper chromosome segregation. Chapter 4 attempts to gain some insight into this process, and focuses on understanding how the activity of two key antagonistic kinesins, present at

the same time, on the same set of microtubules, is coordinated to achieve precise spindle positioning.

Together, these studies have shed light on the mechanistic nuances of how protein function is coordinated to position and disassemble the mitotic spindle, and they present a novel model for how the Ipl1/Aurora B kinase is recruited to the spindle midzone in late anaphase, a process conserved across eukaryotes.

To my parents and my sister

Table of Contents

List of Figures

List of Tables

Abbreviations

AID	auxin-inducible degron
APC	anaphase-promoting complex
ATP	adenosine triphosphate
BME	beta-mercaptoethanol
CPC	chromosomal passenger complex
DMSO	dimethyl sulfoxide
DTT	dithiothreitol
GFP	green fluorescent protein
GTP	guanosine triphosphate
IAA	indole-3-acetic acid
MAPs	microtubule-associated proteins
PBS	phosphate buffered saline
RFP	red fluorescent protein
SDS-PAGE	sodium dodecyl sulfate-polyacrilamide gel electrophoresis
SEM	standard error of the mean
SPB	spindle pole body
TEV	tobacco etch virus
TCA	trichloroacetic acid
TIRF	total internal reflection fluorescence
WT	wild-type
YPD	yeast extract-peptone-dextrose

Acknowledgements

So many people have helped me over the past years at Berkeley. I have learned something from every single one, and I am extremely grateful to all of them. First and foremost I would like to express my sincerest gratitude to my advisors David Drubin and Georjana Barnes for trusting me, and for giving me the opportunity to do my Ph.D at Berkeley, something I would have never imagined would be within my reach. I would also like to thank them for their scientific guidance, constant support and encouragement over all these years. It has really been a dream to do my Ph.D at Berkeley, I have learned so much, and it has impacted my life in so many ways. I certainly wouldn't be the scientist and person I am today if it wasn't for them, and because of that I'll be forever grateful.

I would like to thank my parents Santos and Mari for raising me in a loving and caring environment, and for teaching me the value of persistence and dedication. I also want to thank my sister Nekane for her support and advice to help me keep things in perspective. Living away from home for these past years has been challenging, and I wouldn't have accomplished this, if it weren't for the values that I learned from them, for their constant support, and love. I feel extremely fortunate to belong to this family, and there is simply no way to express my gratitude strongly enough.

I also want to thank present and past members of the Drubin/Barnes lab. David and Georjana have created a unique, collaborative and fun lab environment, that I was privileged to join. I would like to thank Anthony Cormier for introducing me to biochemistry, for his endless patience, and French lessons. Many thanks to Nathaniel Krefman for scientific advice, help with tubulin purification, and gossip sessions in Spanish. Thank you to Michelle Lu for scientific advice, for answering all my "english questions", for being my CrossFit partner, for introducing me to urban dictionary, and for making me laugh until I cried, almost every day. Many thanks to present and past members Rebecca Lu, Yidi Sun, Emily Stoops, Ross Pedersen, Jonathan Wong, Zane Bergman, Daphné Dambournet, Christa Cortesio, Akemi Kunibe, Yansong Miao, Matt Akamatsu, Jessica Marks, and Julian Hassinger for bits of advice and encouragement throughout these past years.

Many thanks to Boehringer Ingelheim Fonds, not only for financial support, but also for believing in me, and for their constant efforts to make of me a better and more complete scientist. Thank you for giving me the opportunity to attend the meetings at Woods Hole and Cold Spring Harbor, and for the whale-watching trip ☺.

During my time at Berkeley I have made invaluable friendships that have been fundamental for helping me keep a healthy balance with lab work, and that I hope will last for many more years to come. Firstly, I cannot express my gratitude strongly enough to Sara

CHAPTER 1
Introduction

1.1 Overview

For successful proliferation, cells need to duplicate and segregate their genetic material equally to the two daughter cells, in a faithful yet efficient way. In order to complete this function, cells have evolved the mitotic spindle, a dynamic macromolecular structure formed from microtubules and other associated proteins. Spindle complexity can vary depending on the organism, but there are many key elements that are conserved across species. In all eukaryotic organisms, spindle microtubules are primarily nucleated from two microtubule-organizing centers, and are arranged as a bipolar array. There are three different types of microtubules that constitute the spindle: interpolar, kinetochore, and astral microtubules. Interpolar microtubules (iMTs) extend towards the cell equator and overlap with microtubules emanating from the opposite pole, forming the spindle midzone. Their main function is to provide support for the spindle. Kinetochore microtubules (kMTs) attach to the kinetochore of chromatids and are essential to capture and segregate chromosomes to opposite poles of the cell during anaphase. Astral microtubules (aMTs) connect the microtubule organizing centers to the cell cortex and are important for positioning the spindle. Proper spindle function is essential, as chromosome missegregation results in aneuploidy, which ultimately can lead to cell death, or to birth defects and cancer in more complex organisms (Weaver and Cleveland, 2006). Therefore, gaining a better understanding of the regulation and function of the mitotic spindle is crucial (for review see Walczak and Heald, 2008).

1.1.1 Microtubule structure and function

There are two intrinsic properties of microtubules that are essential for the function of the spindle: their structural polarity and their intrinsic dynamic behavior. Microtubules are formed by polymerization of α/β-tubulin heterodimers that assemble head-to-tail into a protofilament. Normally 13 protofilaments associate laterally with the same orientation and close into a hollow cylinder that is the microtubule. This creates a structural polarity on the microtubule where the α-tubulin subunits are exposed at one end (termed the minus end) and the β-tubulin subunits are exposed at the opposite end (called the plus end). The ability of many microtubule-associated proteins (MAPs) to recognize this polarity is essential for spindle function. The other important property of microtubules is their inherent dynamic behavior. Microtubules can grow and shrink by addition or loss of tubulin subunits from either end. They can switch stochastically between periods of growth, and sudden shrinkage events termed catastrophes, in a process called dynamic instability (Mitchison and Kirschner., 1984). The dynamics of the ends are different though: the plus end is the fast-growing end, while the minus end is slower. Also, the minus end is capped at the microtubule-organizing center in the cell. Therefore, the plus end seems to be more biologically relevant to the control of microtubule assembly. To orchestrate the different stages of mitosis and ensure faithful chromosome segregation, microtubule-associated proteins tightly regulate the intrinsic dynamic behavior of microtubules.

1.1.2 The mitotic spindle and the cell cycle in budding yeast

Budding yeast is an ideal model organism for studies of the function and regulation of the mitotic spindle because most of the proteins are conserved throughout metazoans, and yeast has the advantage of having a very simple spindle. A key difference from most

other eukaryotes is that yeast cells undergo a closed mitosis, meaning that the nuclear envelope never breaks down. The yeast microtubule-organizing centers, called spindle pole bodies, are embedded in the nuclear envelope and face both the nucleus and the cytosol. Microtubule plus ends are nucleated from the spindle pole bodies and extend toward the interior of the nucleus (nuclear microtubules: iMTs and kMTs) or toward the cytosol (cytosolic/astral microtubules: aMTs). The structure of the yeast spindle is extremely simple. It has approximately 4 iMTs that emanate from each pole and interdigitate with the plus ends of iMTs emanating from the opposite pole, forming the midzone and providing stability to the spindle. There is just one kMTs attached to each centromere, meaning that there are a total of 16 kMTs emanating from each SPB. There are only two to three astral microtubules extending from each SPB. Also, yeast has only two genes that encode α-tubulin, *TUB1* and *TUB3*, and just one gene, *TUB2*, that encodes β-tubulin. The simplicity of its spindle makes budding yeast an excellent organism for studies of microtubule regulation in the cell cycle.

Budding yeast start building the spindle as the cell begins mitosis, in G1 phase. Late in G1, the SPB duplicates and the bud starts to emerge. At this point each SPB has both a set of nuclear and cytoplasmic microtubules. SPB duplication is completed after START, at which point the cell is committed to dividing. There is a G1 checkpoint that triggers cell cycle arrest before proceeding to START if DNA damage is detected or if the cell has not reached the right size. After duplication, the SPBs start to separate and begin to form a bipolar spindle. In S phase the cell duplicates its DNA and the spindle is still short (~600nm). The spindle continues to elongate and the cell then proceeds to G2/M, at which point nuclear microtubules will undergo rapid cycles of polymerization and depolymerization to capture kinetochores, and achieve kinetochore biorientation (Huang and Huffaker, 2006). The metaphase spindle has a length of ~1.5 μm. At this stage there is a second checkpoint called "spindle assembly checkpoint" that ensures that the mitotic spindle is properly assembled and that all kinetochores are bioriented. Once this checkpoint has been satisfied, a signaling cascade activates the anaphase-promoting complex (APC), which in turn promotes degradation of the cohesins that hold sister chromatids together, ultimately allowing chromatid segregation. This event marks the onset of anaphase. Anaphase in yeast is composed of two substages: anaphase A and anaphase B. Sister chromatids are separated to opposite poles of the cell during anaphase A, while during anaphase B chromosomes have already reached the poles and the spindle elongates, reaching a length of up to 10 μm, to further separate the two sets of chromosomes (Maddox et al., 2000). After anaphase has been completed, spindle disassembly starts: microtubule-stabilizing proteins detach from the spindle, and microtubule-destabilizing proteins are activated to break the spindle at its midzone and promote shrinkage of the spindle halves. The actomyosin ring is assembled at the bud neck and cytokinesis begins. Mother and daughter cells are physically separated and both cells begin a new cell cycle.

In recent years much effort has been put toward understanding the earlier stages of mitosis, (i.e., how the spindle is assembled, how kinetochores are captured, and how sister chromatids are segregated). However, recent studies have shown that breaking down the spindle is as important as building it. Complete spindle disassembly is an essential process for cell viability. Cells that fail to completely disassemble the spindle can complete mitosis, but are not able to build a functional spindle in the next cell cycle and eventually die due to chronic arrest (Woodruff et al., 2012). Despite the importance of this process, we still know

very little about how the mitotic spindle is finally broken down. The goal of my PhD thesis is to expand our knowledge about this process. With this goal in mind, I focused on studying the function of the Chromosomal Passenger Complex (CPC), a master regulator of mitosis, whose function during spindle disassembly is essential, yet still not well understood (Buvelot et al., 2003).
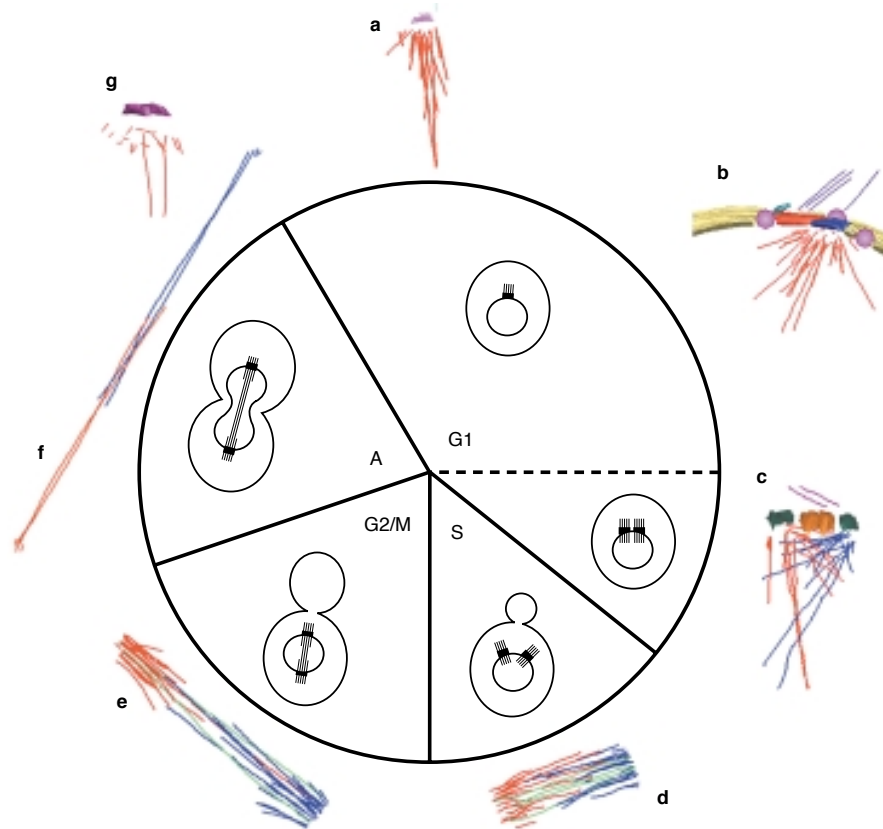
Figure 1.1: The budding yeast cell cycle. The cartoon shows a schematic of how a budding yeast cell progresses through the cell cycle, and more detailed tomography representations of how the mitotic spindle looks at each of the stages. The SPB is shown in pink, the nuclear envelope is yellow, nuclear MTs are red and blue depending on the pole that they emanate from, cytoplasmic MTs are purple and the bridge connecting newly duplicated SPBs is red. Mitosis starts at G1 when the SPB duplicates **(A, B)**. During S phase the SPBs start to separate to form a bipolar spindle **(C, D)** and the DNA duplicates. During G2/M phase the spindle has reached a length of 1-2 μm **(E)**, and kinetochores are bi-oriented. In anaphase sister chromatids are separated and the spindle reaches its maximum length **(F)**, before spindle disassembly and cytokinesis begin, both cells separate and the next cell cycle begins (Figure from Winey and O'Toole, 2001).

1.1.3 The Chromosomal Passenger Complex and its function during mitosis

There are many protein kinases and phosphatases that ensure successful completion of mitosis. One of the most important kinases is Aurora B, or Ipl1 in budding yeast. The Ipl1/Aurora B kinase associates with three regulatory proteins: Sli15/INCENP, Bir1/Survivin, and Nbl1/Borealin, forming a four-subunit complex called the Chromosomal Passenger Complex (CPC). The CPC is conserved across eukaryotes, and the function of each of its subunits is essential for cell survival (Carmena et al., 2009). Guided by the three regulatory subunits, the CPC has a very dynamic localization throughout the cell cycle, which allows the kinase Ipl1 to regulate many key mitotic processes (Murata-Hori et al., 2001). In G1 through early M phase the CPC localizes to chromatin, where it is important for chromatin condensation (Hsu et al., 2000), and for error correction and kinetochore bi-orientation through phosphorylation of the Dam1 complex (Cheeseman et al., 2002; Pinsky et al., 2006). At the onset of anaphase, the CPC translocates to localize all along the mitotic spindle, where it is important for spindle stability (Nakajima et al., 2011). Finally, at the end of anaphase, just before the spindle breaks, the CPC concentrates at the spindle midzone (Cooke et al., 1987), where it is thought to phosphorylate microtubule-stabilizing proteins such as Bim1 to promote their dissociation from the midzone (Zimniak et al., 2009), and to phosphorylate and activate microtubule-destabilizing proteins like She1 (Woodruff et al., 2010) to ultimately promote spindle disassembly. This dramatic change in localization is quick, and probably essential for the spindle to disassemble properly, as late anaphase substrates of Ipl1 localize at the midzone (Buvelot et al., 2003). In my dissertation research I have been particularly interested in understanding how this relocalization happens as a way to broaden our knowledge of how spindle disassembly is triggered, and to eventually gain some insight into how the cell cycle is regulated. From work in mammalian cells we have learned that the kinesin-6 Mklp2 is required for Aurora B to relocalize to the central spindle in anaphase (Gruneberg et al., 2004). However, an important question that remained to be answered from this work was whether the CPC is actually a cargo of Mklp2, or whether the role of Mlkp2 in targeting the CPC to the midzone is not through direct interaction, but rather through an indirect mechanism. Therefore, a more comprehensive understanding of how the CPC is targeted to the midzone was missing prior to this dissertation work. Chapter 2 describes an investigation of the proteins required to target the CPC to the midzone in budding yeast, and also an *in vitro* reconstitution of the process using purified components. By combining cell biology and biochemistry, this dissertation research is able to propose a more detailed mechanism for how the CPC is recruited to the spindle midzone.

Another important question is how this change in CPC localization is achieved by posttranslational modifications. We know that the association of Ipl1 with spindle microtubules and hence its function, is regulated through phosphorylation/dephosphorylation of Ipl1 regulatory subunits by Cdk1/Cdc14 and Ipl1/Glc7 (Nakajima et al., 2011; Zimniak et al., 2012). However, the exact signaling event that triggers CPC recruitment to the spindle midzone is not yet well understood. Cdk1 and Ipl1-mediated phosphorylation of Sli15 prevent the association of the CPC with microtubules during M phase. Spindle microtubules are highly dynamic during M phase to facilitate the establishment of correct microtubule-kinetochore attachments and bi-orientation. Since the CPC is able to stabilize microtubules, it makes sense that there is a mechanism to prevent its binding to the spindle when microtubules need to be dynamic.

During anaphase, Cdc14, the antagonistic phosphatase to Cdk1, is released from the nucleolus and dephosphorylates Cdk1 targets, including Sli15. This allows the CPC to bind and stabilize spindle microtubules, so that they can elongate, and further separate the two sets of chromosomes. Also, the CPC is able to self regulate, as phosphorylation of Sli15 by Ipl1 prevents premature concentration of CPC to the spindle midzone. Nakajima and colleagues proposed that during late anaphase, once the spindle is fully elongated, Glc7-mediated dephosphorylation of Sli15 promotes the recruitment of CPC to the spindle midzone, which would limit microtubule polymerization to prevent spindle overgrowth. We attempted to investigate how Ipl1-mediated phosphorylation of Sli15 regulates the interaction of the CPC with other proteins involved in spindle disassembly, like Kip1. However, our results were not conclusive and further studies need to be done.

1.1.4 Microtubule-binding proteins and their function during mitosis

The dynamics of spindle microtubules change dramatically throughout mitosis. During metaphase microtubules are highly dynamic to allow them to probe the nucleus, find sister chromatids and establish bi-orientation. Once bi-orientation is accomplished, and the cell progresses into anaphase, microtubules become stable, allowing elongation of the spindle. Finally, when chromosomes have reached opposite poles and the spindle has fully elongated, microtubules become unstable and depolymerize to completely disassemble the spindle and start the next cell cycle. To be able to coordinate all the functions of the spindle at the right time, the intrinsic dynamic instability of spindle microtubules has to be precisely regulated. This task is achieved by microtubule-binding proteins. There are two major types of microtubule-binding proteins: motor proteins and non-motor proteins (called MAPs), (see Table 1). As would be expected, many of these proteins are CPC substrates.

1.1.4.1 Microtubule motor proteins

In budding yeast, there are only 6 motors implicated in spindle function: one dynein and 5 kinesin-like proteins. The contribution of those motors to spindle function can be categorized into three fundamental activities: 1) transporting cargoes to a microtubule end, 2) promoting microtubule growth or shrinkage by acting as polymerases or depolymerases at the microtubule end, and 3) cross-linking parallel or anti-parallel microtubules. The motors that operate within the nucleus are Kip1, Cin8, Kip3 and Kar3 and they are important to assemble, elongate and disassemble the spindle. The cytoplasmic motors Kip2, Kip3, Kar3 and Dynein are important for positioning the spindle perpendicular to the division plane. During my dissertation research I have investigated both the mechanisms of spindle positioning and the mechanisms of spindle disassembly. Therefore, to a greater or lesser extent, my dissertation research has studied each of these motors.

Kip1 and Cin8 are exclusively nuclear, kinesin-5 motors, that cross-link and slide antiparallel microtubules apart to generate outward forces that contribute to spindle assembly and elongation. They share strong sequence similarity in their motor domains and have partially overlapping functions (for review see Ferenz et al., 2010). They both have predicted Ipl1-phosphorilation sites. However, whether these sites are biologically relevant and whether they affect their function is still unknown. Chapter 2 describes a screen to determine whether one of the plus end directed nuclear kinesins is responsible for targeting the CPC to the spindle midzone, and identifies Kip1, but not Cin8, as the main motor responsible for the transport of the CPC. Kar3 is antagonistic to Kip1 and Cin8. It is a

minus end directed motor that belongs to the kinesin-14 family. Kar3 is present both in the nucleus and in the cytosol. The current model proposes that the spindle is maintained by a balance of two opposing forces: an outward-directed force exerted by Kip1 and Cin8 that pushes the two SPBs apart, and an inward-directed force provided by nuclear Kar3, which pulls the SPBs together (Saunders and Hoyt., 1992). Kar3 can also function as a microtubule depolymerase in the cytosol, where it is thought to promote microtubule depolymerization to bring the two nuclei together during karyogamy (Molk et al., 2006). Association of Kar3 with either Cik1 or Vik1 light chain regulates Kip3 binding to microtubules and its activity (Sproul et al., 2005). Kip3 is a depolymerase member of the kinesin-8 family (Figure 1.2). It is present in both the nucleus and the cytosol. In the nucleus it is important for kinetochore clustering during metaphase (Wargacki et al., 2010) and for depolymerizing microtubules during spindle disassembly (Woodruff et al., 2010). In the cytosol, it regulates the length of astral microtubules, and it is important for correct positioning of the mitotic spindle (Pearson and Bloom., 2004). Kip2 is a yeast orphan kinesin and is antagonistic to Kip3. It is exclusively cytoplasmic and promotes microtubule growth by increasing the polymerization rate of microtubules and preventing catastrophes (Hibbel et al., 2015; Chapter 3 of this dissertation). Chapter 3 describes an investigation of how the activity of these two antagonistic motors, both present on astral microtubules, is coordinated to achieve proper spindle positioning. Dynein is a minus end-directed motor present in the cytosol, whose only known activity is on astral microtubules, by which it orients the spindle (Carminati and Stearns, 1997).

Figure 1.2: Depolymerase activity of Kip3 on stabilized microtubules. Montage of kymographs of several GMPCPP-stabilized microtubules incubated with 40nM Kip3. Kip3 has a strong microtubule-depolymerase activity. Most of the microtubules were completely depolymerized after 5 min.

1.1.4.2 Microtubule-associated proteins

Microtubule-associated proteins bind to microtubules and regulate their dynamics by different mechanisms: 1) stabilizing and promoting microtubule growth, 2) destabilizing microtubules, or 3) mediating the interaction of microtubules with other proteins or structures. There are specific motifs that mediate the association of MAPs with microtubules. The major ones are the tumor overexpressing gene domain (TOG domain), calponin homology domain (CH domain), and the glycine-rich domain (CAP-GLY domain). Some MAPs such as Bim1/EB1 and Bik1/CLIP170, are conserved in more complex eukaryotes, but there are other ones, like She1, for which an ortholog has not been identified. Bim1 is a plus-end tracking protein present in the nucleus and in the cytosol. Chapter 3 describes how Bim1 on its own promotes microtubule growth by increasing the polymerization rate and preventing catastrophe events. In the nucleus it is present on the midzone, where it is important to stabilize the spindle. During late anaphase nuclear Bim1 is phosphorylated by Ipl1. This causes dissociation of Bim1 from the midzone and promotes spindle disassembly (Zimniak et al., 2009). In the cytosol, Bim1 at the plus ends of microtubules mediates the

interaction of aMTS with Myo2 from the actin cytoskeleton, to ultimately position the spindle adjacent to the bud neck before anaphase (Woodruff et al., 2009). During anaphase, Bik1, which is transported by Kip2, targets dynein to the plus end of aMTs. Once at the plus end, dynein is off-loaded onto the cell cortex of the emerging bud where it pulls the spindle to position it perpendicular to the division plane (McNally, 2013). She1 is another MAP involved in positioning of the spindle. Its function is to restrict dynein activity to anaphase by inhibiting the association of dynein with the dynactin complex before anaphase (Woodruff et al., 2009). She1 is also present in the nucleus, where recent work has shown that it is a microtubule-destabilizing factor involved in spindle disassembly. She1 is phosphorylated and activated by Ipl1 (Woodruff et al., 2010). Chapter 4 describes an investigation of the mechanism by which She1 destabilizes microtubules by using a reconstitution assay to test the effect of purified She1 on microtubule dynamics.

Table 1.1: Spindle parts list (Adapted from Winey and Bloom., 2012)

Protein	Gene	Biological process
α-tubulin	*TUB1* and *TUB3*	MT cytoskeleton as an heterodimer with Tub2
β-tubulin	*TUB2*	MT cytoskeleton as an heterodimer with Tub1 or Tub3
Motors		
Kinesin-5	*KIP1* and *CIN8*	Spindle assembly, elongation, and disassembly
Kinesin-14	*KAR3*	Spindle assembly and orientation, karyogamy
	CIK1	Targets Kar3 to MT plus end, promoting depolymerization, and also spindle orientation
	VIK1	Targets Kar3 to spindle, cross-links spindle MTs
Kinesin-8	*KIP3*	MT depolymerase, involved in spindle orientation and disassembly
Orphan kinesin	*KIP2*	MT polymerase, involved in spindle orientation
Orphan kinesin	*SMY1*	Interacts electrostatically with actin
Dynein	*DHC1*	Minus end motor involved in spindle orientation
MAPs		
EB1	*BIM1*	Spindle stability and orientation
CLIP170	*BIK1*	Spindle orientation
CLASP	*STU1*	Spindle stability
XMAP215	*STU2*	Dynamicity factor
PRC1	*ASE1*	Spindle stability and spindle elongation
Orphans	*SHE1*	Spindle-destabilizing factor, spindle orientation
	IRC15	Chromosome orientation, checkpoint

CHAPTER 2

Transport of the Chromosomal Passenger Complex to the spindle midzone by Kip1 and Kip3 is essential for efficient spindle disassembly

2.1 Abstract

Disassembling the mitotic spindle after chromosomes have separated is as important as building it, but the molecular mechanisms for spindle disassembly are unclear. Complete spindle disassembly is essential for cell viability: cells that cannot completely disassemble the spindle can exit mitosis but are unable to build a functional spindle in the next cell cycle (Woodruff et al., 2012). The Chromosomal Passenger Complex (CPC) is a master regulator of mitosis and is required for efficient spindle disassembly. In late anaphase, the CPC quickly re-localizes from being all along the spindle to being concentrated at the spindle midzone, where it inhibits microtubule growth factors such as Bim1, and activates microtubule destabilizing proteins such as She1 to initiate spindle disassembly (Zimniak et al., 2009; Woodruff et al 2009). How the CPC swiftly concentrates at the spindle midzone just before spindle breakdown is not yet understood. In this study, we determined whether a plus end-directed kinesin is responsible for the transport of the CPC to the spindle midzone during late anaphase. We showed that the kinesins Kip1 and Kip3 are essential for CPC to localize to the midzone. Cin8, the motor with some functional overlap with Kip1, does not play an important role during this process. Bim1, a well known midzone protein, is able to localize normally to the midzone in *kip1Δ kip3 Δ* mutant cells, indicating that failure of the CPC to localize properly is not due to a general problem with the midzone. We also found that if the CPC cannot localize to the midzone, spindle disassembly is severely delayed, and as a result the spindle stays intact even after disassembly of the cytokinetic ring. We reconstituted the relocalization process *in vitro* with microtubules and purified CPC-GFP and Kip1. We found that CPC-GFP alone is able to bind microtubules, and to diffuse on them. However, upon addition of Kip1, the amount of CPC-GFP bound to microtubules increases dramatically, suggesting that Kip1 directly interacts with the CPC and is able to recruit it to microtubules. Single molecule experiments show that the CPC is able to move directionally towards the microtubule end in the presence of Kip1, suggesting that Kip1 is transporting it. We propose that Kip1 is the main kinesin responsible for CPC midzone localization. During late anaphase, Kip1 is able to interact with the CPC and transport it to the spindle midzone. Our results also suggest that the CPC needs to be at the midzone to be able to phosphorylate midzone proteins such as Bim1 and She1, and ultimately facilitate spindle breakage and disassembly.

2.2 Introduction

The Aurora B kinase (Ipl1 in budding yeast) is part of the Chromosomal Passenger Complex (CPC), which associates with mitotic spindle microtubules and is one of the master regulators of mitosis (for review see Shannon et al., 2002). The CPC is conserved across eukaryotes and has a very dynamic localization throughout mitosis, which allows it to regulate different stages of this process (Figure 2.1; Petersen et al., 2001; Murata-Hori et al., 2002). How the CPC dynamically changes its localization to coordinate mitotic progression is still poorly understood.

In order to orchestrate the different stages of mitosis and ensure the fidelity of chromosome segregation, the intrinsic dynamic behavior of microtubules needs to be regulated. This task is accomplished by several microtubule-associated proteins, some of which are targets of the CPC (Hsu et al., 200; Cheeseman et al., 2002; Kotwaliwale et al., 2007; Zimniak et al., 2009; Woodruff et al., 2010). Microtubule dynamics change significantly

as mitosis progresses: microtubules are highly dynamic around metaphase to facilitate kinetochore capture, then become stable during anaphase to elongate the spindle and further separate chromosomes, and finally they are highly unstable to allow disassembly of the spindle. Historically, research has mostly focused on understanding the earlier stages of mitosis. However, recent studies have highlighted the importance of proper spindle disassembly. Very little is still know about how cells are able to swiftly and efficiently disassemble the spindle, even though it is an essential process for cell viability (Woodruff et al., 2012). The spindle midzone is of especial importance during spindle disassembly, since is the region where the spindle breaks to initiate disassembly. There is a subgroup of microtubule-associated proteins that localize at the spindle midzone (Winey et al., 2001). These proteins include both motor and non-motor proteins (Howard and Hyman, 2007; Khmelinskii et al., 2008). Their function at the midzone is mainly to stabilize the overlapping region of antiparallel microtubules (e.g., Bim1, the budding yeast homolog of EB1, and Ase1, budding yeast PRC1), and to drive spindle assembly and power anaphase by generating an outwardly directed force (e.g., the kinesin-5 motors Kip1 and Cin8) that pushes the microtubule organizing centers (spindle pole bodies in yeast) apart (Saunders and Hoyt., 1992). However, we don't fully understand what, if any, is their precise role during spindle disassembly.

In late anaphase the CPC is known to participate in two processes. The first is spindle disassembly, which it regulates by phosphorylating and inactivating the microtubule-stabilizing protein Bim1, leading to its dissociation from the midzone and hence destabilizing the spindle (Zimniak et al., 2009). Ipl1 phosphorylation of the microtubule-destabilizing protein She1 is also important for efficient spindle disassembly (Woodruff et al., 2009). The second process regulated by the CPC is the NoCut pathway, a checkpoint that ensures that chromosomes have cleared the plane of division before cytokinesis starts (Norden et al., 2006). Just before the onset of spindle disassembly, the CPC dramatically changes its localization from being along the length of the spindle, to concentrating at the midzone, where it presumably performs its functions to promote spindle disassembly and mitotic exit (Figure 2.1, Buvelot et al., 2003). This relocalization happens swiftly and is not well understood. Since the spindle midzone is formed by overlapping microtubule plus-ends that emanate from opposite poles, a possible mechanism could be that the CPC gets transported to the midzone by a plus-end directed kinesin. From work in mammalian cells, we know that the kinesin Mklp2 is required for CPC midzone localization (Kitagawa et al., 2013). However, despite the importance and highly conserved nature of this relocalization, whether it happens through direct interaction and transport, or through an indirect mechanism, is not known. In budding yeast, there are only four nuclear kinesins, namely Kip1, Kip3, Cin8 and Kar3. However, only Kip1, Kip3, and Cin8 are plus-end directed, and so, these are good candidates to transport the CPC to the spindle midzone.

Spindle disassembly is an essential process (Woodruff et al., 2012). However, very little is known about how it is regulated. In this study, we combined cell biology with biochemistry and biophysical approaches to investigate the role of the CPC during spindle disassembly. We describe the role of the different nuclear kinesins during spindle disassembly and propose a model for how the CPC gets targeted to the spindle midzone to promote spindle disassembly.
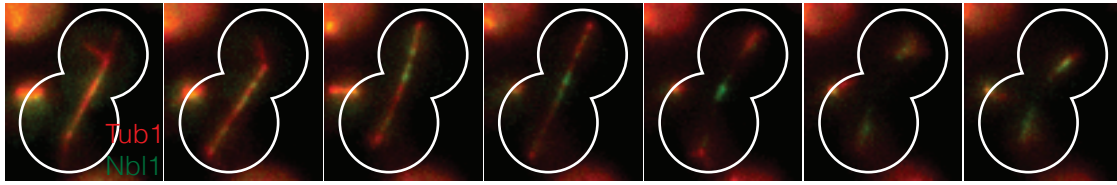
Figure 2.1: Localization of the CPC during late anaphase. Cells expressing Tub1-mCherry and Nbl1-GFP are undergoing anaphase. In early anaphase the CPC localizes all along the spindle, where it is important for spindle stability. In late anaphase, the CPC quickly concentrates to the spindle midzone. How this swift change in localization happens is still poorly understood. The goal of this project is to elucidate the mechanisms how this relocalization is achieved.

2.3 Results

2.3.1 The CPC co-localizes with all three plus end nuclear kinesins during late anaphase

The spindle midzone is formed by plus ends of bundled microtubules that emanate from opposite spindle poles. Therefore, nuclear plus end-directed kinesins are good candidates to transport the CPC toward the spindle midzone. In budding yeast, three different plus-end directed kinesins are present in the nucleus: Cin8, Kip1 and Kip3.

To determine whether any of these kinesins might transport the CPC to the midzone, we first examined the localization of each motor and the CPC during late anaphase. We labeled the Nbl1 subunit of the CPC with an mCherry tag, and expressed it with either GFP-labeled Cin8, Kip1 or Kip3 to look for co-localization. Indeed, consistent with previous studies (Fridman et al., 2013), Kip1 localizes to the spindle midzone in late anaphase and follows the plus ends of depolymerizing microtubules upon spindle breakage, co-localizing with Nbl1 throughout late anaphase and spindle disassembly (Figure 2.2 C, D). Similarly, Kip3 also co-localizes with Nbl1 at the spindle midzone in late anaphase. However, upon spindle breakage, in contrast to the CPC, Kip3 did not follow the ends of depolymerizing interpolar microtubules (Figure 2. 2E, F). Cin8 did dimly co-localize with Nbl1 at the spindle midzone and, similar to Kip1, also tracked the ends of shrinking microtubules (Figure 2.2 A, B). In summary, all three nuclear kinesins co-localize with the CPC in the midzone during late anaphase, but only Kip1 and Cin8 track the depolymerizing microtubules together with the CPC upon spindle breakage.
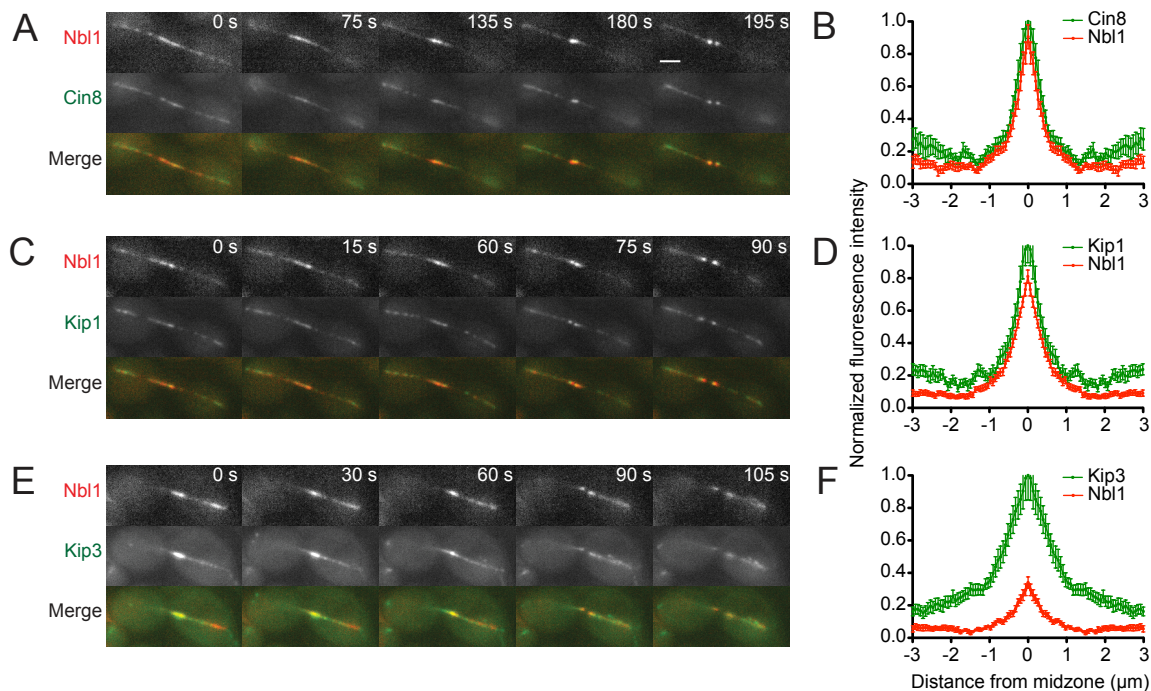
Figure 2.2: All three plus end directed nuclear kinesins co-localize with the CPC at the spindle midzone during late anaphase. (A, C and E) Time-lapse of representative yeast cells expressing Nbl1-mCherry (top rows), and either Cin8-GFP, Kip1-GFP, or Kip3-GFP, respectively, (middle rows). The bottom rows show a merged image of Nbl1-mCherry (red) and Cin8-GFP, Kip1-GFP, or Kip3-GFP (green). Cells are undergoing late anaphase and spindle disassembly. Time in seconds is shown on the top right corner. Scale bar is 2 μm. **(B, D and F)** Quantification of fluorescence intensity along the spindle on the frame just before the onset of spindle disassembly. Graphs show normalized spindle fluorescence versus distance from the midzone in μm, where the value "0" represents the spindle midzone. Red graph is fluorescence intensity of Nbl1-mCherry, and green is fluorescence intensity of Cin8-GFP, Kip1-GFP, or Kip3-GFP along the spindle midzone. Error bars are standard error of the mean.

2.3.2 Kip1 is required for robust CPC midzone localization

To determine which of the nuclear kinesins might recruit the CPC to the spindle midzone, we analyzed CPC localization in mutants of each of the nuclear kinesins. We specifically looked at cells expressing Nbl1-GFP to follow the CPC, and Tub1-mCherry to be able to see the spindle, in combination with *kip1Δ*, *cin8Δ* or *kip3Δ* mutations. We looked at a mixed population of wild-type and mutant strains in each trial to directly compare fluorescence intensities. To distinguish between wild-type and mutant strains (*kip1Δ*, *cin8Δ* or *kip3Δ*), the wild-type strain expressed the spindle pole body protein Spc42 labeled with mCherry in addition to Nbl1-GFP and Tub1-mCherry (Figure 2.4 A). To ensure that the Spc42-mCherry did not affect our quantification, we compared the localization of the CPC in a strain expressing Tub1-mCherry and a strain expressing Tub1-mCherry Spc42-mCherry. The amount of CPC in the midzone was not significantly different in the two strains,

indicating that the Spc42-mCherry marker would not affect our quantification. We compared Deletion of *CIN8* did not have any detectable effect on CPC localization at the midzone. However, deletion of *KIP1* decreased CPC midzone localization by almost 50%, and deletion of *KIP3* decreased it by over 20% (Figure 2.4 B-E).

2.3.3 Kip1 and Cin8 requirement for spindle elongation during anaphase can be rescued by *kar3Δ*.

Cin8 and Kip1 are known to be partially redundant motors (Hoyt et al., 1992; Cui et al., 2009). Our results so far indicate that Kip1 is the motor primarily responsible for CPC midzone localization. However, in *kip1Δ* cells some CPC is still concentrated at the midzone. Therefore, we hypothesized that Cin8 might be able to provide some Kip1 function during late anaphase when the latter is absent. This would explain why the CPC is partially localized to the spindle midzone in a *KIP1* null strain. To address this possibility, we generated a strain deficient in both *KIP1* and *CIN8*. The presence of at least one of the motors is essential for viability, so we created an auxin-inducible degron mutant of Cin8 (CIN8-AID*) that allows rapid Cin8 degradation upon addition of auxin to the growth media, and combined it with a *kip1Δ* mutation. Immunoblotting confirmed that Cin8 is reduced to almost undetectable levels upon treatment with 250 μM indole-3-acetic acid (IAA, a type of auxin) for 15 min (Figure 2.4 J). To determine whether Cin8 function is abolished, we compared growth of *kip1Δ* CIN8-AID* cells with wild type cells and single mutants on plates with IAA. *kip1Δ* CIN8-AID* cells grow as well as wild type cells on YPD plated containing DMSO. However, they die on YPD plates containing IAA, indicating that the degron is working and the function of Cin8 is indeed abolished (Figure 2.4 I). To observe the morphology of the spindle of *kip1Δ* CIN8-AID* cells, cells were arrested with alpha factor, released into imaging media and watched until they entered anaphase, at which point 250 μM IAA was added to the media. The cells also expressed Tub1-mCherry, which allowed us to monitor spindle length and follow entry into anaphase. Wild-type spindles reached a full anaphase length about 1.5 hours after release from alpha factor, and started disassembly when they reached a length of 9.4 μm. In contrast, 1.5 hours after release from alpha factor, *kip1Δ CIN8-AID** spindles had not reached full anaphase length yet. Most of these cells were large budded but had short spindles that were not able to reach full length and ended up breaking prematurely at an average length of 7 μm (Figure 2.3 B). The fact that all short spindles eventually break without completing anaphase is consistent with the spindle being sheared by contraction of the acto-myosin ring and membrane ingression. This result indicates that cells lacking both Kip1 and Cin8 function, can still progress into cytokinesis even though is has not yet completed anaphase. These observations support the idea that Kip1 and Cin8 are required for spindle elongation during late anaphase.

In order to determine whether Cin8 and Kip1 play redundant functions in late anaphase to transport the CPC to the midzone, we needed a way for cells to be able to fully elongate the spindle in the absence of both motors. The structure of the mitotic spindle is maintained by counteracting pushing and pulling forces generated by Cin8/Kip1 and Kar3, respectively. Previous studies have shown that deletion of Kar3 suppresses the temperature-sensitivity of *cin8-3 kip1Δ* (Hoyt et al., 1992; Hoyt et al., 1993). Similarly, deletion of *KAR3* in the *kip1Δ CIN8-AID** strain, rescued the lethality of the double mutant (Figure 2.4 I). It also rescued the short spindle phenotype, as the average spindle length before spindle breakdown

in the triple mutant, *kip1Δ kar3Δ CIN8-AID**, in the presence of IAA, was 8.8 μm, close to the average wild-type length (Figure 2.3 B). These results confirm that both Kip1 and Cin8 are required for spindle elongation during anaphase, and that Kar3 counteracts their pushing force.
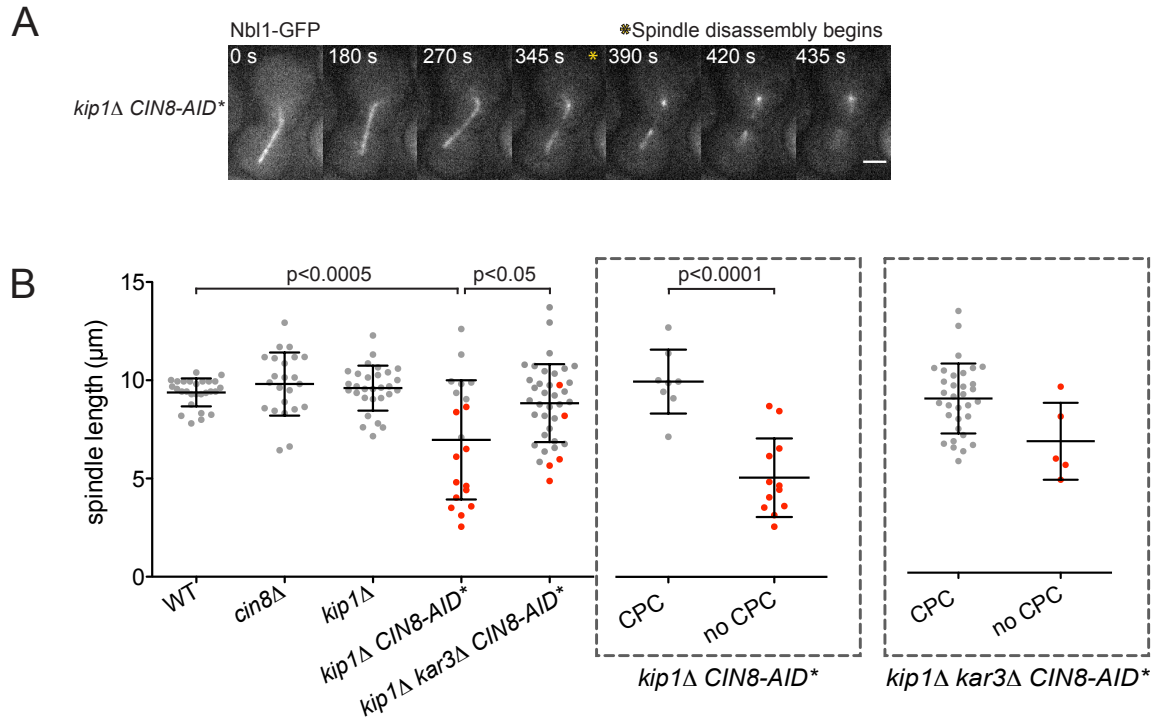
Figure 2.3: Cin8 and Kip1 are required for spindle elongation during anaphase. (A) Time-lapse of a representative *kip1Δ CIN8-AID* cell expressing Nbl1-GFP. Time of each frame is shown in seconds on the top right corner of each image. Yellow star marks the frame when the spindle breaks. Scale bar is 2μm. **(B)** Quantification of spindle length at the frame when the spindle breaks. Grey dots are cells in which the CPC is at the midzone when the spindle breaks, while red dots are cells in which the CPC is not concentrated at the midzone at the time when the spindle breaks. Errors bars are standard error of the mean. First dashed square is *kip1Δ CIN8-AID** strain and second is *kip1Δ kar3Δ CIN8-AID** strain. Data points were separated depending on whether the CPC was concentrated at the midzone (grey dots) or not (red dots) at the time of spindle breakage.

2.3.4 Neither Cin8 nor Kar3 is required to concentrate the CPC at the midzone

In wild-type cells, the CPC decorates the midzone just before the spindle breaks and then it follows the depolymerizing ends of microtubules. However, in *kip1Δ CIN8-AID** cells, whose spindles break without elongating, the CPC evenly decorates the entire length of the spindle and is not concentrated at the midzone at the time when the spindle breaks (Figure 2.3 A). At least two possible reasons why the CPC is not being recruited to the midzone exist. One possibility is that it cannot get to the midzone because both Kip1 and

Cin8 are required to transport it there. Another possibility is that a structure or signaling event required for this process is only present in long anaphase spindles and not in the early anaphase spindles of the double mutant. To distinguish between these possibilities, we analyzed CPC localization on long anaphase spindles of the triple *kip1Δ kar3Δ CIN8-AID** mutant. The CPC was able to localize to the midzone of these cells to a similar extent as in single *kip1Δ* cells (Figure 2.4 G). This result suggests that Cin8 and Kar3 are not required to concentrate the CPC at the spindle midzone, and that Kip1 plays a unique role in this process.

Our data so far shows that deletion of *KIP1* causes a 50% reduction of the amount of CPC concentrated in the spindle midzone. This also means that in the absence of Kip1, some CPC can still be recruited to the midzone. We have also observed that additional deletion of two more nuclear kinesins (Kar3 and Cin8) does not significantly reduce the amount of CPC recruited to the midzone, suggesting that neither Cin8 nor Kar3 are important for this process.

2.3.5 CPC localization at the spindle midzone is dependent on Kip1 and Kip3.

Interestingly, deletion of *KIP3* only, caused a mild reduction in the amount of CPC recruited to the midzone (Figure 2.4 E). We therefore decided to combine a *kip1Δ* with a *kip3 Δ*. Strikingly, in the absence of both Kip1 and Kip3, the CPC was completely unable to concentrate at the spindle midzone (Figure 2.4 H). However, this dramatic reduction might be a consequence of midzone defects caused by the absence of the two motors. To address this possibility and to determine whether this defect also affects other midzone proteins, we analyzed localization of a well known midzone protein, Bim1, in the absence of both Kip1 and Kip3. Bim1 localizes normally to the spindle midzone of *kip1Δ kip3Δ* cells, and it tracks the ends of depolymerizing microtubules upon spindle breakage, as in wild-type cells (Figure 2.5 A). This result establishes that there is a functional midzone in *kip1Δ kip3Δ* cells, but that CPC cannot localize there, suggesting that indeed Kip1 and Kip3 are required to recruit the CPC to the midzone. Given that *kip1Δ kip3Δ* cells are alive, this result also suggests that the localization of the CPC to the midzone is not essential for life or spindle disassembly.
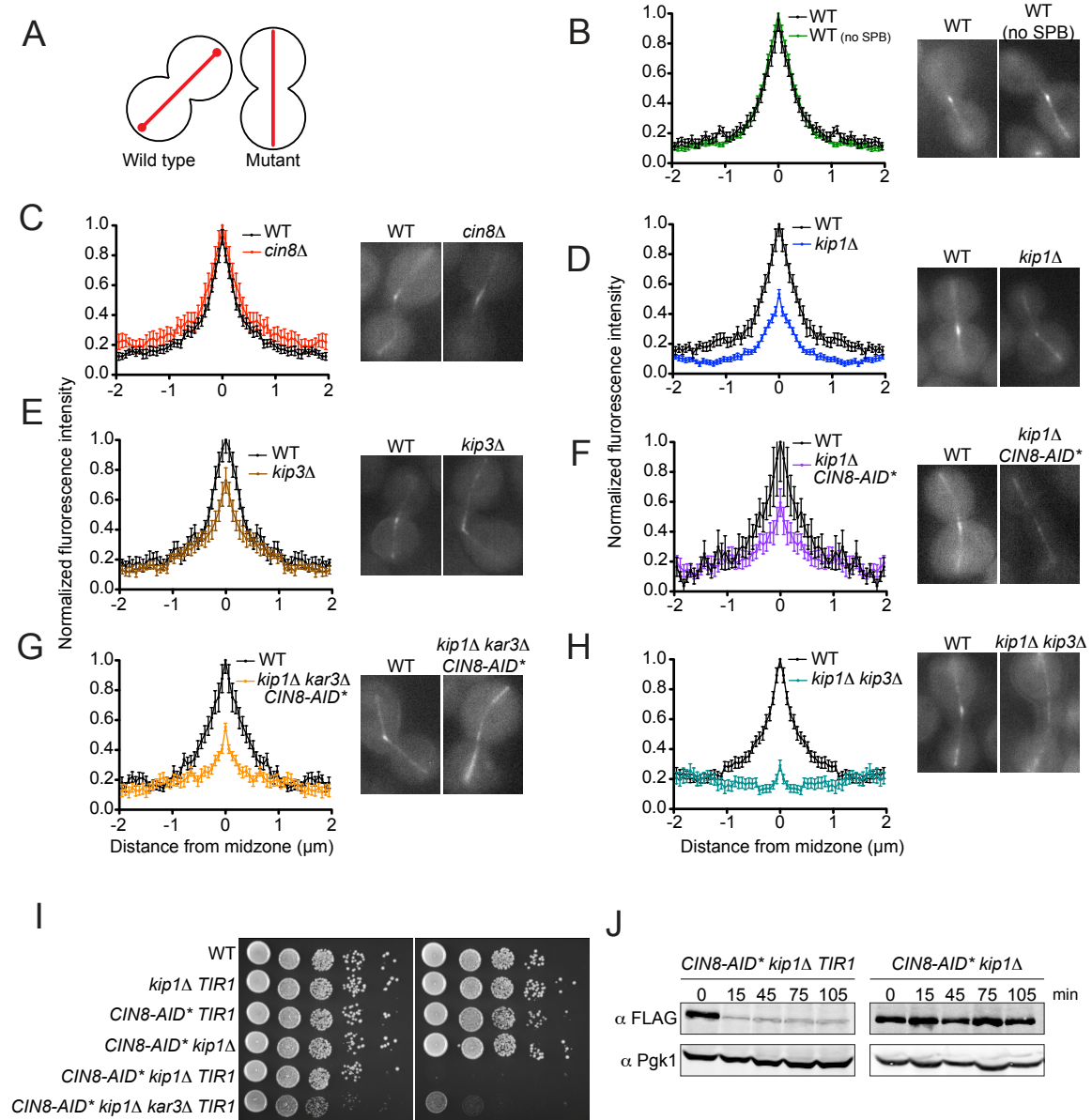
Figure 2.4: The CPC cannot concentrate at the spindle midzone when Kip1 and Kip3 are both absent. (A) Schematic of the experimental design: To be able to compare fluorescence intensities of wild-type and mutant strains, cells were mixed and observed on the same coverglass. Both WT and mutants expressed Nbl1-GFP and Tub1-mCherry, but WT also expressed Spc42-mCherry, which allowed us to distinguish between the WT and the mutant. **(B - H)** Graphs show normalized fluorescence intensity versus position on the spindle for WT (black line) and each of the mutants or WT control (varying colors) on the frame just before the onset of spindle disassembly. Error bars are standard error of the mean. Images on the right of each graph show representative WT or mutant cells that express Nbl1-GFP. All images shown are the frame just before the onset of spindle disassembly. **(I)** Growth assay to assess the viability of the *kip1Δ CIN8-AID** strain. Five different dilutions of each of the strains were spotted onto two plates: mock (YPD + DMSO) and YPD + 250μM IAA. Degradation of Cin8 is dependent on *TIR1*. IAA is Indolacetic Acid, AID is

17

Auxin-inducible degron. **(J)** Time-course of *kip1Δ CIN8-AID* TIR1* and *kip1Δ Cin8-AID* strains to determine timing of Cin8 degradation. The first sample was taken 15 min after addition of IAA to the growth media, and the next time points were taken every 30 min.
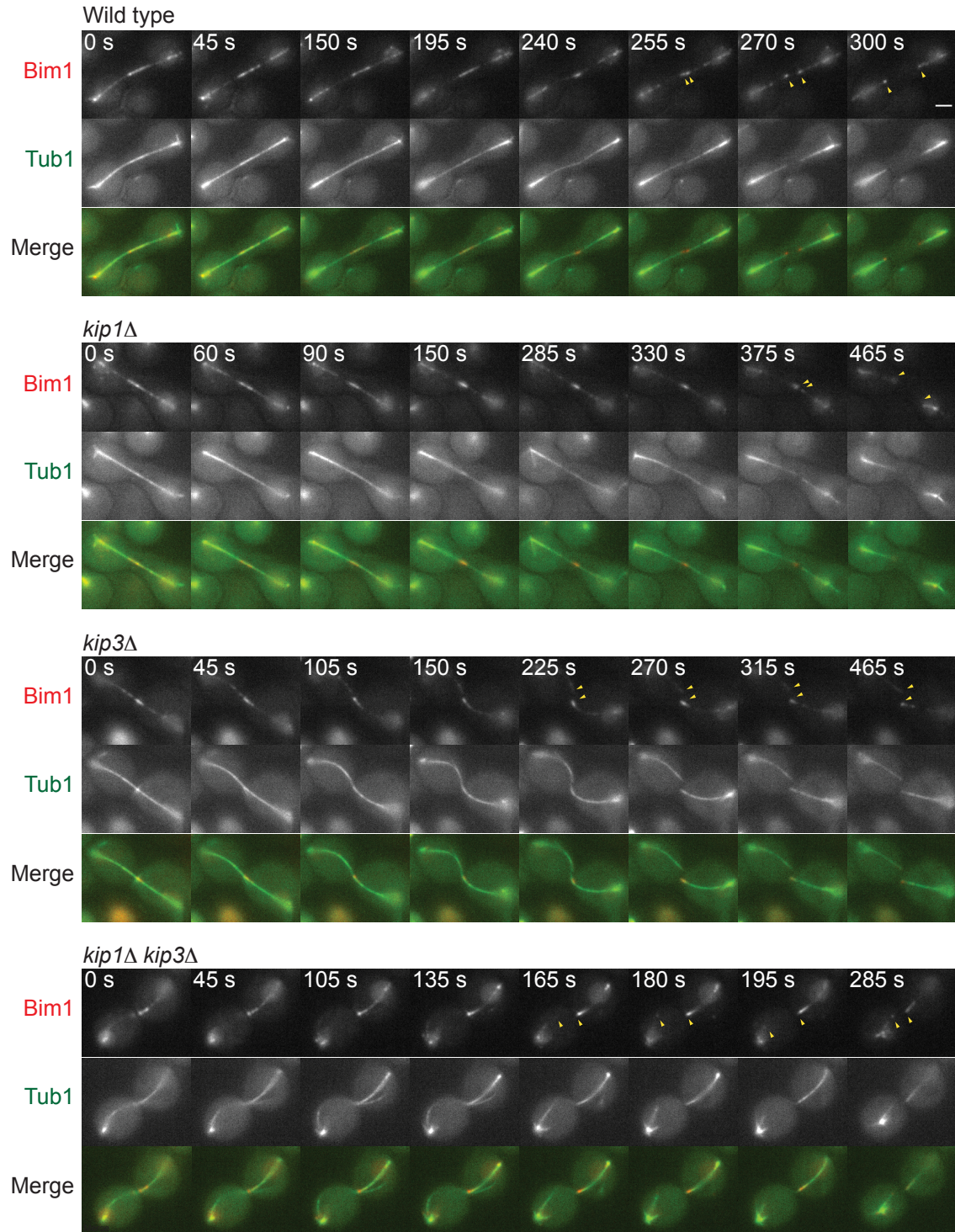
Figure 2.5: Bim1 can still localize to the spindle midzone in the absence of Kip1 and Kip3. (A) Time-lapse of WT, *kip1Δ*, *kip3Δ* or *kip1Δ kip3Δ* representative cells expressing Bim1-tagRFPt and Tub1-GFP. Cells were imaged from late anaphase through spindle disassembly. Yellow arrowheads indicate depolymerizing spindle ends. Time in seconds is shown on the top right corner. Scale bar is 2 μm.

2.3.6 CPC midzone localization is required for timely spindle disassembly

Previously it was shown that the budding yeast Aurora B subunit of the CPC, Ipl1, is required for efficient spindle disassembly (Buvelot et al., 2003, Woodruff et al., 2010). To determine whether the CPC midzone localization is required for efficient spindle disassembly, we analyzed this process in *kip1Δ kip3Δ* cells. We used Myo1-EGFP to follow contraction of the cytokinetic ring, and GFP-Tub1 to determine when the spindle breaks relative to the time when the cytokinetic ring starts to contract. In wild-type cells the spindle breaks before the cytokinetic ring has finished constriction (Figure 2.6 A). The same relative timing was observed in *kip1Δ* single mutants (Figure 2.6 A). In agreement with previous studies (Woodruff et al 2010), *kip3Δ* mutants exhibit delayed spindle disassembly, as the spindle only breaks when the cytokinetic ring has almost finished contraction. Strikingly, the spindle of *kip1Δ kip3Δ* double mutants stays unbroken long after the cytokinetic ring has contracted and the Myo1 ring has disassembled (Figure 2.6 A-C). These results show that both Kip1 and Kip3 are required for timely spindle disassembly, and suggest that this defect might be a consequence of CPC not being able to concentrate at the spindle midzone.

2.3.7 The spindle breakage delay in *kip1Δ kip3Δ* cells is not a consequence of the NoCut pathway remaining active

It has been shown that spindle midzone defects lead to a delay in abscission through the NoCut pathway. This pathway ultimately ensures that cytokinesis only proceeds once all the chromosomes have cleared the plane of division, and depends on Ipl1 and the anillin-related proteins Boi1 and Boi2 (Norden et al 2006). We hypothesized that the delayed spindle disassembly phenotype in *kip1Δ kip3Δ* cells might be a result of the CPC not being able to concentrate at the midzone and not being sequestered away from chromatin, thereby holding the NoCut pathway active and delaying cytokinesis. To test this hypothesis, we analyzed Boi1 and Boi2 localization. In wild-type cells, Boi1 and Boi2 localize to the bud neck during anaphase and relocate into the nucleus after spindle breakdown. Ndc10 is a midzone protein required for midzone stability. *ndc10-1* mutants are defective in cytokinesis and Boi1 stays at the bud neck even after a new bud emerges (Norden et al 2006). However, in *kip1Δ kip3Δ* mutants, Boi1 and Boi2 exhibit the same localization as wild-type cells (Figure 2.7 B,C). Deletion of *BOI1* and *BOI2* was reported to rescue the abscission delay of *ase1Δ* cells (Norden et al 2006). However, deletion of *BOI1* and *BOI2* in the *kip1Δ kip3Δ* strain did not rescue the delay in spindle disassembly (Figure 2.6 A,C). All together, these results suggest that the delay in spindle disassembly observed in *kip1Δ kip3Δ* cells is not a consequence of the NoCut pathway remaining active. Thus, Kip1 and Kip3 are likely directly required for efficient spindle disassembly.
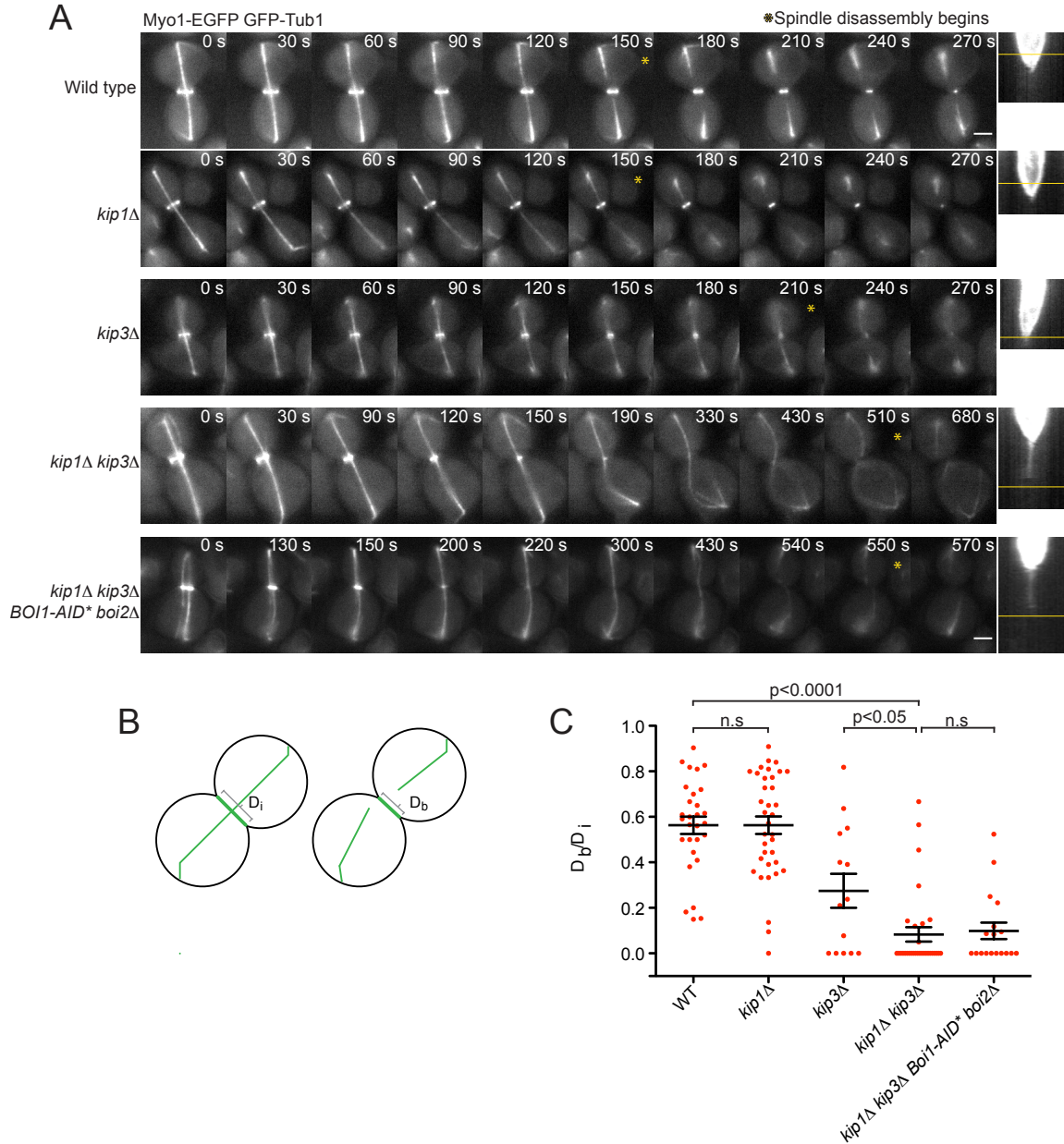
Figure 2.6: *kip1Δ kip3Δ* cells exhibit severely delayed spindle disassembly. (A) Time-lapse of a WT, *kip1Δ*, *kip3Δ*, *kip1Δ kip3Δ* and *kip1Δ kip3Δ Boi1-AID* boi2Δ* cells expressing Tub1-GFP and Myo1-GFP. Cells undergo anaphase followed by spindle disassembly. The yellow star marks the point when the spindle breaks. Time in seconds is shown in the top right corner of each image. Scale bar is 2 μm. The corresponding kymograph showing contraction of the cytokinetic ring is shown to the right of each time-lapse series. On each kymograph, the yellow line indicates the frame in which the spindle breaks. **(B)** The cartoon represents a cell expressing Tub1-GFP and Myo1-GFP and shows the diameter of the ring before it has started to contract (D_i) and the diameter of the ring when the spindle breaks (D_b). **(C)** Quantification of D_b/D_i for each of the strains shown. Error bars are standard error of the mean.

21
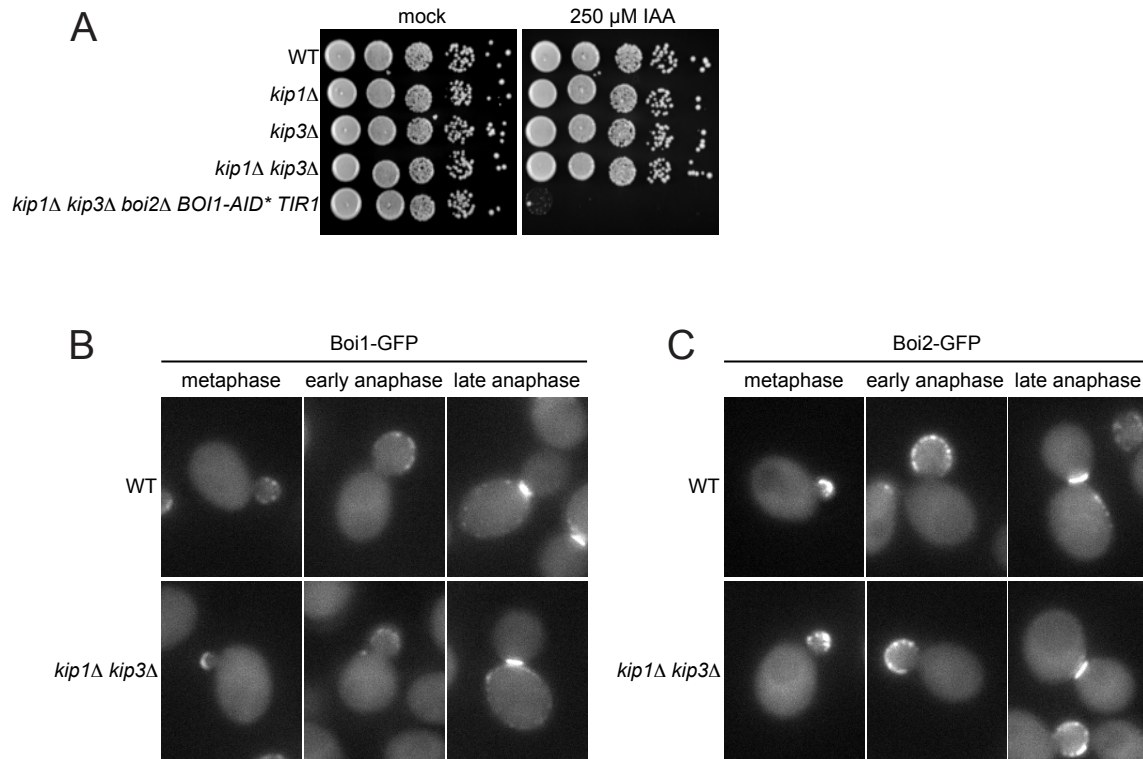
Figure 2.7: The NoCut pathway does not stay active in the absence of Kip1 and Kip3.
(A) Growth assay to assess viability of the *kip1Δ kip3Δ Boi1-AID* boi2Δ* strain. Five different dilutions of each of the strains were spotted onto two plates: mock (YPD + DMSO) and YPD + 250μM IAA. IAA is Indolacetic Acid, AID is Auxin-inducible degron. *kip1Δ kip3Δ Boi1-AID* boi2Δ* cells die in the presence of auxin in the growth media. **(B and C)** WT and *kip1Δ kip3Δ* cells expressing Boi1-GFP (b) or Boi2-GFP (c) that are undergoing metaphase, early anaphase or late anaphase. The localization of neither Boi1 nor Boi2 changes in the absence of Kip1 and Kip3.

22

2.3.8 Kip1 directly recruits Nbl1-GFP to microtubules *in vitro*

To determine whether the effect of Kip1 on CPC localization is through a direct interaction between these proteins or through an indirect mechanism, we purified Kip1 and also the 4-subunit CPC labeled with a GFP tag on its Nbl1 subunit (CPC-GFP). We polymerized microtubules out of a mixture of unlabeled, biotin-labeled and rhodamine-labeled porcine tubulin and fixed them to a streptavidin-coated coverglass. CPC-GFP alone was able to bind rhodamine-labeled microtubules with low efficiency. However, in the presence of Kip1, the amount of CPC-GFP present on microtubules dramatically increased when compared to CPC-GFP with microtubules alone (Figure 2.8 A). These data show that Kip1 interacts directly with the CPC and recruits it to microtubules. Next, we wanted to investigate whether Kip1 would also be able to transport the CPC to one of the microtubule ends. We reduced the amount of CPC-GFP and Kip1 in the assay to be able to observe the behavior of single CPC-GFP molecules in the presence of Kip1. To reduce photobleaching, and have a brighter signal that would allow us to track the movement of single CPC-GFP molecules, we attached a quantum dot to CPC-GFP. In the presence of Kip1, we observed some diffusive movement, but we also saw some molecules moving with directionality towards one of the microtubule ends (Figure 2.8 B). All together, these results suggest that Kip1 interacts with the CPC directly, recruits it to the microtubule, and indeed, transports it to the microtubule end.
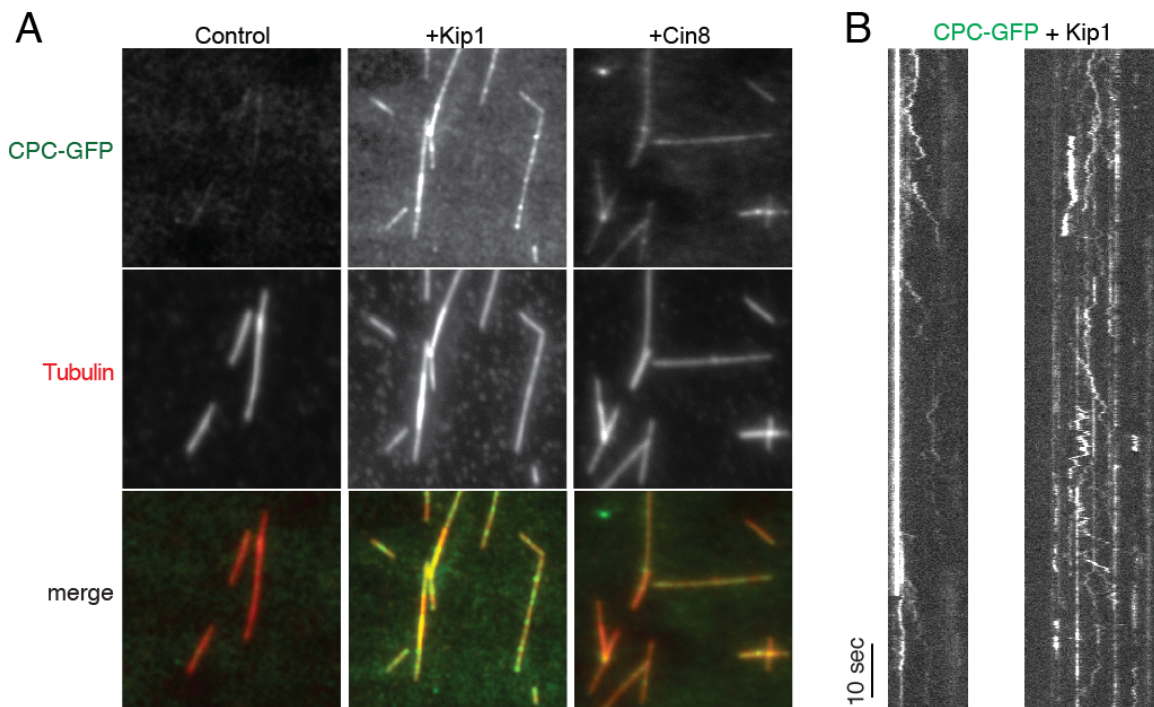
Figure 2.8: Kip1 interacts with the CPC and recruits it to microtubules *in vitro*. (A) Purified CPC-GFP (Bir1, Sli15, Ipl1 and Nbl1-GFP-6xHis) was added to immobilized rhodamine-labeled microtubules in the absence of motors (Control), in the presence of Kip1 (+Kip1), or in the presence of Cin8 (+Cin8) **(B)** Kymographs of CPC-GFP moving on microtubules in the presence of Kip1.

2.4 Discussion

The CPC is a central regulator of distinct stages of mitosis, whose finely choreographed changes in localization underlie its ability to perform its functions. Here we focused on the mechanism by which the CPC relocalizes from the entire length of the spindle to the spindle midzone late in anaphase. Because microtubules in the spindle are oriented with their plus-ends toward the cell center, we hypothesized that the CPC might be transported to the midzone by a plus-end directed nuclear kinesin.

Budding yeast offers the advantage of having a closed mitosis, which limits which proteins can be involved in the process, and also has the advantage of having only 4 nuclear kinesins, 3 of which are plus-end directed (namely Kip1, Kip3 and Cin8). In this study we determined which of the nuclear kinesins, if any, is responsible for concentrating the CPC to the spindle midzone just before the onset of spindle disassembly. We found that the kinesin Kip1 is required for robust CPC recruitment to the spindle midzone during late anaphase. Strikingly, in the absence of both Kip1 and Kip3, CPC midzone localization was almost completely abolished. The two other nuclear kinesins (Cin8 and Kar3) do not play a significant role in recruiting the CPC to the spindle midzone, even though Cin8 is known to have partially overlapping functions with Kip1. However, this has been observed in other processes too: Kip1 but not Cin8 is required for localization and equal segregation of the 2-micron plasmid in budding yeast (Cui et al., 2009). The defect in CPC recruitment to the spindle midzone is not a consequence of a defective spindle midzone resulting from the absence of Kip1 and Kip3, since the midzone protein Bim1 is able to concentrate normally at the midzone in a *kip1Δ kip3Δ* strain. This observation demonstrates that the defect is specific for the CPC and suggests a more direct relationship between Kip1/Kip3 and the CPC. Since our cell biology data indicated that Kip1 might be the main kinesin responsible for CPC midzone localization, we decided to focus our attention on Kip1 to further investigate the recruitment mechanism. We reconstituted the system using purified components in an *in vitro* TIRF assay. Our results indicate that Kip1 interacts directly with the CPC and recruits it to microtubules, and that indeed, in the presence of Kip1, CPC molecules can directionally move towards the microtubule end. All together, our results demonstrate that CPC can be transported by Kip1 to the spindle midzone. The fact that Kip3 is required in addition of Kip1 for recruitment of CPC to the midzone *in vivo*, but that deletion of Kip3 alone does not cause any significant defect in the localization of CPC suggests that Kip1 and Kip3 function together for efficient targeting of CPC. A scenario could be that Kip3 is creating a structure at the midzone that facilitates the attachment of the CPC. In this scenario, in the absence of Kip1, the CPC would be able to diffuse and stay attached to the midzone if Kip3 is present. In the absence of Kip3, Kip1 transports the CPC but it would stay bound less efficiently to the midzone. And in the absence of both motors, the CPC is not efficiently transported to the midzone, and the molecules that do reach the midzone by diffusion, cannot stay bound because of the absence of Kip3. An alternative explanation could be that Kip3 normally is not involved in the recruitment of the CPC to the midzone, but will if Kip1 is absent.

Having a way to prevent the CPC from concentrating at the spindle midzone in late anaphase allowed us to study the role of CPC's midzone localization. Previous studies showed that Ipl1 kinase activity is required for timely spindle disassembly (Buvelot et al., 2003). Zimniak et al showed that phosphorylation of the spindle-stabilizing protein Bim1 by Ipl1 promotes Bim1 dissociation from the midzone and is also required for efficient spindle

disassembly. Therefore, we wondered whether the CPC needs to be at the spindle midzone for timely and efficient spindle disassembly. We found that spindles do not disassemble in a timely manner in the *kip1Δ kip3Δ* mutant and remain intact even after disassembly of the cytokinetic ring. We believe that the spindle can remain unbroken because there is still a narrow cytoplasmic bridge left after disassembly of the actomyosin ring (Norden et al., 2006). Eventually spindles in the double mutant do break but this probably is a consequence of the final cell abscission, since the spindles always break at the bud neck. This result demonstrates that general Ipl1 activity is not enough to drive efficient spindle disassembly; it also needs to be present at the spindle midzone to ensure timely disassembly. Disassembly might be inhibited by a failure of inactivation of the NoCut pathway as a consequence of either CPC not being sequestered away from chromatin to the spindle midzone or because of midzone defects caused by the CPC not being present at the midzone (Norden et al., 2006). We knocked out Boi1 and Boi2, which are believed to act downstream of Ipl1 to delay abscission. We expected that this would silence the NoCut pathway and the cell would now be able to exit mitosis normally. However, spindle disassembly defects were not rescued in the *kip1Δ kip3Δ BOI1-AID boi2Δ* mutant. This result suggests that spindle disassembly is inhibited through a different mechanism than the NoCut pathway.

We also confirmed that both Kip1 and Cin8 are required for spindle elongation during anaphase. Previous studies showed that both kinesins generate an outwardly directed force that balances the pulling force exerted by Kar3 during spindle assembly. By using a temperature-sensitive allele of Cin8 in a *kip1Δ* strain they were able to show that the microtubule-organizing centers were duplicated but unable to separate, and therefore that both proteins are required for assembly of the mitotic spindle. It has also been shown that both kinesins are also required following spindle assembly, since preanaphase bipolar spindles collapse when the function of both proteins was compromised. However, until now it was believed that anaphase spindles are resistant to collapse and that Kip1 and Cin8 are no longer required during anaphase. By using the auxin-inducible degron system, we have shown that, indeed, both proteins are still required during anaphase. In their absence, the anaphase spindle cannot elongate, however the cell is still able to enter cytokinesis, which eventually breaks the short anaphase spindle. Cytokinesis allows the daughter cells to separate, but probably compromises chromosome segregation. We were able to rescue the short spindle phenotype of the double Cin8-AID *kip1Δ* mutant by deleting Kar3. This result supports the idea that the reason why the spindle cannot elongate is because of the lack of the Kip1/Cin8-supplied force to counteract Kar3, and demonstrates that overcoming the pulling forces exerted by Kar3 is required for spindle elongation during anaphase.

The goal of this study was to gain a better understanding of how cells finish mitosis and how the onset of spindle disassembly is regulated. We focused on understanding how the Aurora B complex, the CPC, swiftly concentrates to the spindle midzone just before spindle disassembly begins and on investigating its function at the midzone. We found that Kip1 is the main motor responsible for CPC midzone localization, and our results suggest that this is achieved by directed transport towards the microtubule plus ends. Once at the spindle midzone, the CPC is essential to trigger spindle disassembly. The spindle can still be broken even if Our results provide a model for how spindle disassembly is regulated by the CPC. Since all the components are conserved, we expect our results to be applicable to more complex eukaryotes.

2.5 Materials and methods

2.5.1 Strain culture and construction

All yeast strains used in this study are S288c derivatives and are listed in Table 2.1. Yeast were grown in yeast extract/peptone (YP) media with 2% glucose unless otherwise noted. To generate fluorescent protein fusions and gene deletions we followed standard methods of PCR followed by yeast transformation and recombination (Longtine et al., 1998). To generate the auxin- inducible degron strains, we used the plasmids described on Morawska and Ulrich., 2013.

For the serial dilution assay, cells were grown overnight in YPD to saturation, and diluted to OD_{600} 1 the next morning. We then made 5 sets of 10 fold dilutions and spotted 4µl of each dilution onto agar plates. Cells were grown at the indicated temperatures for 48 hours before imaging.

2.5.2 Protein purification

CPC-GFP, CPC (WT) and CPC (17A) were purified essentially as reported (Cormier et al., 2013).

For purification of Kip1, plasmid pIZ62 was transformed into IZ32. Overnight precultures were used to inoculate 2 liters of synthetic medium supplemented with 2% raffinose and dropout Uracil and Leucine and grown for 16 hours at 30ºC. Cultures were induced with 2% galactose for 9 hours, harvested by centrifugation, drop frozen and lysed using a 6870 Freezer/Mill (SPEX SamplePrep, Metuchen, NJ). Cell powder was thawed in 2x lysis buffer (100mM NaH_2PO_4 pH 7.5, 1M KCl, 1mM ATP, 5mM $MgCl_2$, 20mM BME, 2% Triton, 20% glycerol, 80mM Imidazole pH 7.5, 2mM PMSF and 2x Complete Protease Inhibitor Cocktail without EDTA (Roche)), centrifuged for 30 min at 85,000 rpm in a Beckman TLA100.3 rotor (Beckman Coulter) at 4ºC. Clarified lysate was injected into a HisTrap HP column (GE Healthcare), washed with Wash buffer (50mM NaH_2PO_4 pH 7.5, 500mM KCl, 0.1mM ATP, 1mM $MgCl_2$, 10mM BME, 1% Triton, 10% glycerol, 40mM Imidazole pH 7.5, 1mM PMSF and 1x Complete Protease Inhibitor Cocktail without EDTA (Roche)) and eluted using a gradient of Elution buffer (50mM NaH_2PO_4 pH 7.5, 250mM KCl, 0.1mM ATP, 1mM $MgCl_2$, 10mM BME, 10% glycerol and 1M Imidazole pH 7.5). Elution fractions containing Kip1 were pooled together and the buffer was exchanged to Final buffer (50mM NaH_2PO_4 pH 7.5, 250mM KCl, 0.1mM ATP, 1mM $MgCl_2$, 10mM BME, 20% glycerol) using a PD10 desalting column (GE Healthcare). At this step, Kip1 was incubated with 6xHis-TEV protease overnight at 4º. The next morning, Kip1 containing 6xHis-TEV was incubated with 500µl of Ni-NTA agarose (ThermoFisher Scientific) for 2h at 4ºC and centrifuged for 1min at 1000 g to separate the resin containing 6xHis-TEV from the supernatant with Kip1. The supernatant was collected, concentrated using an Amicon centrifugal filter unit (EMD Millipore), aliquoted and flash frozen in liquid N_2.

For purification of Kip3, plasmid pIZ69 was transformed into a IZ32. Used an overnight preculture to inoculate 2 liters of synthetic medium supplemented with 2% raffinose and dropout Uracil and Leucine and grown for 16 hours at 30ºC. Cultures were induced with 2% galactose for 10 hours, harvested by centrifugation, drop frozen and lysed using a 6870 Freezer/Mill (SPEX SamplePrep, Metuchen, NJ). Cell powder was thawed in 2x lysis buffer (100mM Hepes pH 7.5, 1M KCl, 1mM ATP, 10mM $MgCl_2$, 2mM DTT, 2%

Triton, 20% glycerol, 80mM Imidazole pH 8, 2mM PMSF and 2x Complete Protease Inhibitor Cocktail without EDTA (Roche)), centrifuged for 30 min at 85,000 rpm in a Beckman TLA100.3 rotor (Beckman Coulter) at 4°C. Clarified lysate was injected into a HisTrap HP column (GE Healthcare), washed with Wash buffer (50mM Hepes pH 7.5, 200mM KCl, 0.5mM ATP, 5mM MgCl$_2$, 1mM DTT, 1% Triton, 10% glycerol, 40mM Imidazole pH 8, 1mM PMSF and 2x Complete Protease Inhibitor Cocktail without EDTA (Roche)) and eluted using a gradient of Elution buffer (50mM Hepes pH 7.5, 200mM KCl, 0.5mM ATP, 5mM MgCl$_2$, 1mM DTT, 1% Triton, 10% glycerol and 1M Imidazole pH 8). Elution fractions containing Kip3 were pooled together and incubated with 6xHis-TEV protease overnight at 4°. The next morning, we used a PD10 desalting column (GE Healthcare) to exchange the buffer to Low salt buffer (50mM Hepes pH 7.5, 100mM KCl, 0.5mM ATP, 5mM MgCl$_2$, 1mM DTT, 1% Triton and 10% Glycerol) and the protein was bound to a HiTrap Capto Q (GE Heathcare) and eluted using a gradient of High salt buffer (50mM Hepes pH 7.5, 1M KCl, 0.5mM ATP, 5mM MgCl$_2$, 1mM DTT, 1% Triton and 10% Glycerol). Kip3 and 6xTEV eluted at different salt concentrations. Elution fractions that contained Kip3 were pooled together and the buffer was exchanged to Final buffer (50mM Hepes pH 7.5, 200mM KCl, 0.5mM ATP, 5mM MgCl$_2$, 1mM DTT, 1% Triton and 10% Glycerol) using a PD10 desalting column (GE Healthcare). The protein was concentrated with an Amicon centrifugal filter unit (EMD Millipore), aliquoted and flash frozen in liquid N$_2$.

2.5.3 Live-cell imaging

For live-cell microscopy, cells were grown to log phase at 25°C in imaging media (synthetic complete medium lacking tryptophan and with 2% glucose) and immobilized on Concanavilin A-coated 25mm round #1.5 coverslips. For imaging of cells during anaphase, cells were synchronized in G1 using alpha factor, and released into imaging media containing pronase. 1.5 hours after release from alpha factor cells were undergoing early anaphase. For imaging of strains with an AID tag, 250μM Indolacetic acid (IAA) was added to the imaging media 1.5 hours after release from alpha factor. Imaging was started after 15 min of incubation with IAA. Movies were taken at 10 sec intervals. Each frame of the movie represents a maximum intensity projection from a z-stack containing 3 planes 0.4μm apart. Images were processed using ImageJ software.

Images were obtained using a Nikon Eclipse Ti microscope (Nikon Instruments, Melville, NY) controlled by MetaMorph (Molecular Devices, Sunnyvale, CA), and equipped with a Plan Apo VC 100x/1.4 Oil OFN25 DIC N2 objective, a MOV-2000 piezo stage (Applied Scientific Instrumentation, Eugene, OR), a Perfect Focus System (Nikon), a temperature-controlled enclosure (InVivo Scientific, St. Louis, MO), and a Neo sCMOS camera (Andor Technology Ltd., South Windsor, CT).

2.5.4 Time course and immunoblotting

To determine the timing of IAA-dependent Cin8-AID* degradation, IZ88A and IZ100 precultures were diluted to OD$_{600}$ 0.1 in imaging media (synthetic medium lacking tryptophan and with 2% glucose) and 250μM IAA was added. An equal amount of cells was harvested for every time point during the 120 min time-course. Cells were immediately TCA precipitated and an equal amount of cell extract was loaded into all lanes (0.5 OD/lane). The

cell extracts were subjected to SDS-PAGE and immunoblot analysis using mouse anti-FLAG (Sigma) and mouse anti-Pgk1 (Invitrogen) antibodies.

2.5.5 *In vitro* binding assay and TIRF microscopy

20x20 1.5# glass coverslips were cleaned by sonication in an isopropanol bath for 20 min, followed by illumination with oxygen gas plasma for 5 min. Clean coverslips were coated with PLL-PEG and PLL-PEG-Biotin, washed with water and PBS, dried using compressed dry nitrogen, and stored in a sealed container at 4°C for up to two weeks. Microtubules were polymerized out of combination of unlabeled tubulin, biotin-labeled tubulin and rhodamine-labeled tubulin (Cytoskeleton) and stabilized with GMPCPP.

For the experiment, a flow chamber was assembled using the functionalized coverslips, a glass slide, and double-sided tape. Channels were incubated with Neutravidin, followed by Pluronic, and then preassembled microtubules. Microtubules stayed bound to the coverslip through biotin-streptavidin interactions. CPC-GFP or CPC-GFP with Kip1 were flown into the flow chamber, incubated for 5 min, and unbound proteins were washed off with BRB80 buffer.

Images were recorded taken using an Olympus IX81 microscope, equipped with a TIRF system, a 100x/1.45 NA oil objective (PlanApo; Olympus) and a sCMOS Flash 4.0 camera (Hamamatsu Photonics).

2.5.6 Quantitative analysis of spindle midzone fluorescence

The frame just before the spindle starts to disassemble was identified from each of the movies, and adjusted to the same brightness and contrast parameters. We traced a line along the entire length of the spindle to quantify the fluorescence intensity values of each pixel. The same line was moved parallel to the spindle to quantify background fluorescence and subtract it from the values of the spindle. The values were then corrected for photo bleaching based on which frame of the movie the spindle began disassembly. To prevent any bias based on the orientation of the spindle, we made the fluorescence intensity values for each spindle symmetric by inverting the intensity values of each spindle and averaging them. Spindles were aligned at the pixels where the spindle breaks.

Table 2.1 Yeast strains used in this study

Strain name	Mating type	Genotype
IZ036	*MATa*	*CIN8-GFP::KanMX NBL1-mCherry::HIS3 leu2-3,112 lys-801 his3Δ200 ura3-52*
IZ184	*MATa*	*KIP1-GFP::KanMX NBL1-mCherry::HIS3 leu2-3,112 lys-801 his3Δ200 ura3-52*
IZ185	*MATa*	*KIP3-GFP::HIS3 NBL1-mCherry::HIS3 leu2-3,112 lys-801 his3Δ200 ura3-52*
IZ061	*MATa*	*NBL1-GFP::KanMX6 TUB1-mCherry::URA3 SPC42-mCherry::KanMX leu2-3,112 lys-801 his3Δ200 ura3-52*
IZ008	*MATa*	*NBL1-GFP::KanMX6 TUB1-mCherry::URA3 leu2-3,112 lys-801 his3Δ200 ura3-52*
IZ016	*MATa*	*cin8Δ::KanMX NBL1-GFP::KanMX TUB1-mCherry::URA3 leu2-3,112 lys-801 his3Δ200 ura3-52*
IZ056	*MATa*	*kip1Δ::HIS3 NBL1-GFP::KanMX TUB1-mCherry::URA3 leu2-3,112 lys-801 his3Δ200 ura3-52*
IZ103	*MATa*	*kip3Δ::HIS3 NBL1-GFP::KanMX6 TUB1-mCherry::URA3 leu2-3,112 lys-801 his3Δ200 ura3-52*
IZ088A	*MATa*	*CIN8-AID*-6FLAG::pHyg TIR1::LEU2 kip1Δ::HIS3 NBL1-GFP::KanMX TUB1-mCherry::URA3 leu2-3,112 lys-801 his3Δ200 ura3-52*
IZ100	*MATa*	*kar3Δ::ClonNAT CIN8-AID*-6FLAG::pHyg TIR1::LEU2 kip1Δ::HIS3 NBL1-GFP::KanMX TUB1-mCherry::URA3 leu2-3,112 lys-801 his3Δ200 ura3-52*
IZ32	*MATa*	*lys2::Pgal1:GAL4::lys2 pep4::HIS3 bar1::hisG ade2 leu2 his3 trp1 ura3*
IZ151	*MATa*	*kip1Δ::HIS3 NBL1-GFP::KanMX TUB1-mCherry::URA3 SPC42-mCherry:KanMX leu2-3,112 lys-801 his3Δ200 ura3-52*
IZ153	*MATa*	*kip1Δ::HIS3 kip3D::HIS3 NBL1-GFP::KanMX TUB1-mCherry::URA3 leu2-3,112 lys-801 his3Δ200 ura3-52*

Table 2.2 Plasmids used in this study

Plasmid name	Description
pIZ03	*pST39: Sli17/Ipl1/Bir1/Nbl1-GFP-His*
pIZ01	*pST39: Sli17/Ipl1/Bir1/Nbl1-His*
pDD2397	*pST39: Sli17 (17A)/Ipl1/Bir1/Nbl1-His*
pIZ69	*Gal-Kip3-TEV-Strep-His*
pIZ62	*Gal-Kip1-TEV-Strep-His*

CHAPTER 3
Analysis of She1 function during spindle disassembly

3.1 Abstract

Spindle microtubules dynamically assemble and disassemble and their accurate regulation by microtubule associated proteins (MAPs) is essential for spindle function. She1 is a yeast protein that helps position the spindle and it has also been linked to spindle disassembly. Yeast cells depleted of She1 are unable to break down the spindle. These spindles eventually shear when the actomyosin ring contracts, but the two remaining spindle halves disassemble at slower rates. These two phenotypes, together with the fact that She1 localizes to the mitotic spindle during anaphase, suggest that She1 could promote spindle disassembly by directly destabilizing spindle microtubules. To gain a better understanding of She1 function during spindle disassembly, we sought to answer the following questions: 1) Does She1 interact with microtubules directly? 2) Does purified She1 affect microtubule dynamics? 3) How does phosphorylation by Ipl1/Aurora B affect She1's activity? Our results showed that purified She1 can interact with taxol-stabilized microtubules directly. However, it didn't seem to have a strong effect on microtubule dynamics. Nor did a constitutively active She1, wherein the five Ipl1 consensus sites were mutated to aspartic acid. Although we learned a lot about She1 biochemistry and its interaction with microtubules, we could not show that it is able to directly destabilize microtubules. Our results instead suggest that She1 promotes spindle disassembly through an indirect mechanism. Furthermore, we identified a novel She1 interacting partner, Mes1, which co-purifies with equimolar stoichiometry, and investigated its relationship with She1.

3.2 Introduction

As described on Chapter 2 of this dissertation, proper spindle disassembly is an essential process for cell viability. Cells that fail to completely disassemble their spindle can still finish mitosis and undergo cytokinesis. However, the two daughter cells are unable to build a functional spindle in the next cell cycle and eventually die due to chronic arrest (Woodruff et al., 2012). Spindle disassembly is a very fast process compared to spindle assembly, and there are at least three parallel pathways that ensure that it is successfully completed. In the first pathway the anaphase-promoting complex (APC) ubiquitinates Ase1, Cin8 and other MT-stabilizing proteins for degradation, promoting separation of the two spindle halves. In a second pathway, the kinesin-8 Kip3 actively drives depolymerization of spindle microtubules. The third pathway is governed by the Ipl1 kinase, which phosphorylates and releases Bim1 from microtubules, therefore destabilizing the midzone, and it also phosphorylates and activates the microtubule-destabilizing factor She1.

She1 is present in both the nucleus and the cytoplasm, and appears to have several functions. In G1 phase it localizes to aMTs where it inhibits the interaction of dynein with dynactin until anaphase, therefore restricting dynein activity until the onset of anaphase ("late" spindle orientation pathway). In early M phase it localizes to kinetochores and to the bud neck (Woodruff et al., 2009), while during anaphase it is present on iMTs, where its involved in spindle disassembly. Cells lacking She1 rely on contraction of the cytokinetic ring to break the spindle, and once it is broken, the spindle halves shrink at a reduced rate compared to wild type cells. Because of these defects and the fact that She1 localizes along the mitotic spindle, it has been suggested that it directly regulates microtubules dynamics (Woodruff et al., 2010). However, the mechanism by which She1 destabilizes microtubules is not yet known. Preliminary experiments done by Jeff Woodruff and described in his

dissertation (Woodruff, 2011) show that purified GST-She1 can bind to microtubules, and that it can also inhibit the growth of microtubules nucleated from purified centrosomes.

The goal of this project was to better understand the contribution of She1 to spindle disassembly, and more specifically, to test whether She1 alone has microtubule-destabilizing activity, similar to the microtubule depolymerase Kip3. We optimized the purification of She1, characterized it biochemically, and quantified its effect on microtubule dynamics. Furthermore, we identified a novel She1 interacting partner, Mes1, which co-purifies with equimolar stoichiometry, and investigated its relationship with She1.

3.3 Results

3.3.1 Optimization of She1 purification

Experiments done by Jeff Woodruff showed that She1 purified from *E. coli* requires a GST tag for solubility (Woodruff, 2011). However, GST is known to dimerize and it is possible that it alters She1 function by inducing dimerization. Our initial approach was to develop a protocol to purify She1 from budding yeast cells, with the idea that She1 might require specific posttranslational modifications in yeast to stay soluble. We generated a yeast expression plasmid driven by the GAL1 promoter, and containing the *SHE1* ORF followed by a 3x Streptavidin and a 9x His tag (pIZ14). We performed a screen to find the optimum induction time and temperature, and also the optimum lysis buffer, by trying a range on different buffers (Tris, Pipes, Hepes, SSC and MES), pH (ranging from 5.5 to 9), and salt concentrations, among other conditions. We found that the best lysis buffer was Tris pH 8.0, 500mM KCl with addition of 10% Glycerol and 50 mM Arg/Glu. However, even in this buffer, 80% of the She1-strep-his remained in the pellet fraction after high-speed centrifugation of the crude lysate. The purification of She1 using the remaining supernatant fraction did not yield high amounts of purified protein. We therefore decided to purify She1 from bacteria, but using a tag that doesn't dimerize. We used a protocol from the Lee lab at UMass to purify She1 labeled with a HALO tag (She1-HALO), and also the constitutively active phosphomimetic She1 (She1$_{5D}$-HALO) from bacteria. We followed the published protocol, and added a size exclusion chromatography step to remove some contaminants (Figure 3.1). Analysis of the UV absorbance profile from the size exclusion column revealed that purified She1-HALO has an apparent molecular mass of 107 kDa, assuming the conformation of a globular protein. The expected molecular weight of She1-HALO is 72 kDa. Therefore this result indicates that purified She1-HALO is a monomer with an elongated shape.
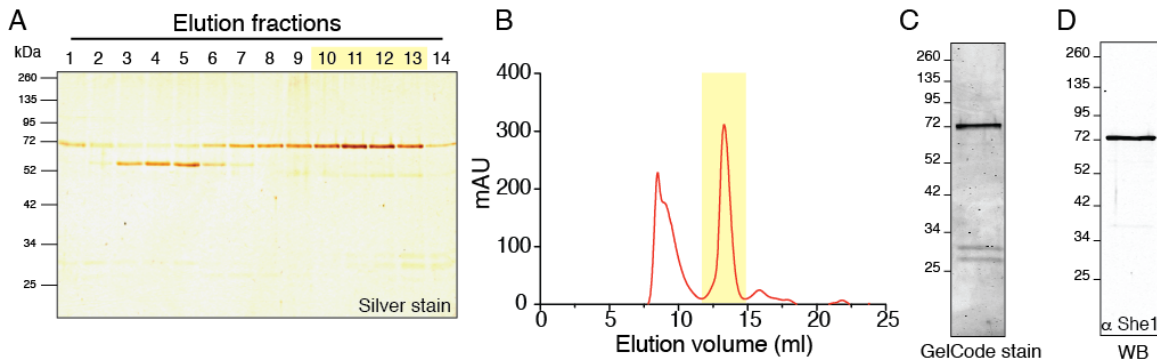
Figure 3.1: Purification of She1-HALO. (A) Silver stained gel of elution fractions from the size exclusion column. Fractions 10-13 (yellow region) were pooled and concentrated. **(B)** UV absorbance profile of elution fractions from size exclusion column as a function of elution volume. The yellow region corresponds to the She1-HALO peak (fractions 10-13 from the silver stain). **(C)** SDS-PAGE gel stained with GelCode showing the final protein after concentration of the fractions from the gel filtration. **(D)** Western blot of final concentrated fractions probed with an anti-She1 antibody. Purification of She1$_{5D}$-HALO produced a very similar elution profile from the size exclusion column.

3.3.2 She1-HALO alone is able to bind microtubules *in vitro*

In cells, She1 associates with aMTS and iMTs microtubules. To test whether She1 alone is able to bind microtubules or whether it requires another protein to mediate its binding, we performed a microtubule cosedimentation assay in which purified She1-HALO was incubated with increasing concentrations of taxol-stabilized microtubules. The results of the titration experiment yielded a K_D of 0.1 μM (Figure 3.2 A, C). To investigate the nature of this interaction, we repeated the sedimentation assay with a higher salt concentration. An increased salt concentration will disrupt electrostatic interactions but stabilize the hydrophobic ones. We found that the calculated K_D at a higher salt concentration increased to 0.5 μM, indicating that the binding of She1 to microtubules is sensitive to high ionic strength. Together, these data demonstrate that She1 alone is able to bind directly to microtubules with moderate affinity, and that this interaction is of electrostatic nature.
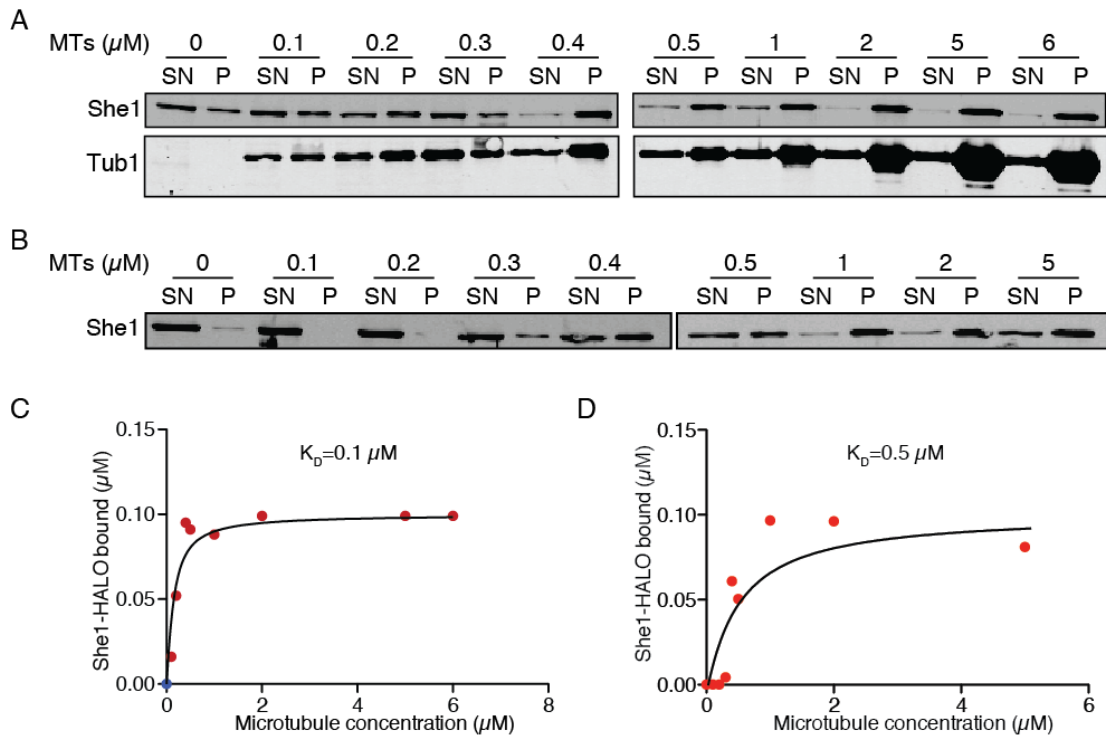
Figure 3.2: She1-HALO binds to microtubules *in vitro* (A) Cosedimentation of 100 nM She1-HALO with varying concentrations of taxol-stabilized microtubules at low salt concentration (35 mM KCl) **(B)** Cosedimentation of 100 nM She1-HALO with varying concentrations of taxol-stabilized microtubules at higher salt concentration (100 mM KCl) (SN, supernatant; P, pellet) **(C)** Bound She1-HALO plotted against the concentration of microtubules in low salt conditions (35 mM KCl) **(D)** Bound She1-HALO plotted against the concentration of microtubules in low salt conditions (100 mM KCl).

3.3.3 Mes1 is a novel She1 interacting partner

In order to investigate whether She1 is also a monomer in the cell, as it is when purified from bacteria, or whether it oligomerizes or forms a complex with other proteins, we performed size exclusion chromatography analysis of yeast cell extracts. Such yeast extracts were prepared as previously described (Sun et al., 2015), separated by gel filtration and the eluted fractions were analyzed by immunoblotting (Figure 3.3 A). By comparing the elution volume when She1 comes off of the size exclusion column (fractions 12 and 13 on Figure 3.3 A), with the elution volume for protein standards of known molecular mass, we calculated that the molecular mass of She1 in the yeast cell extract ranges between 200 and 370 kDa. The molecular size of She1-HALO is ~72 kDa. Therefore, She1 in the cell either oligomerizes or forms a complex with other proteins.

When we performed the purification of She1 from budding yeast cells, we tried two different affinity tags (7.5x myc tag and a 3x Streptavidin-9x His tag) in order to choose the one that yielded more protein. In both purifications She1 co-purified with another protein of higher molecular weight. Strikingly that interacting protein had the same molecular weight in both purifications (~80 kDa), suggesting that it could be the same protein (Figure 3.3 B, C).

35

Mass spectrometry analysis performed by the Yates laboratory at Scripps revealed that the band that co-purifies with She1-strep-his is Mes1. Mes1 is a methionyl-tRNA synthetase that forms a complex with two other proteins (Gus1 and Arc1). However, no mitotic function for Mes1 has been identified. Quantification of the intensity of the bands indicated that She1-strep-his and Mes1 co-purify at an equimolar ratio. To gain additional insight into the interaction between She1 and Mes1 we labeled endogenous Mes1 with a GFP tag and looked at its localization. She1 localizes to both cytoplasmic and nuclear microtubules and also to the bud neck. Mes1, however, was present diffusely in the cytosol and didn't seem to localize on microtubules. To further investigate the relationship between Mes1 and She1, we generated a *Mes1-GPF she1Δ* strain that allowed us to study whether the localization of Mes1 depended on She1. Fluorescence microscopy revealed that the localization of Mes1-GFP looked the same in the presence and in the absence of She1 (Figure 3.3 E), suggesting that Mes1 localization is independent of She1.
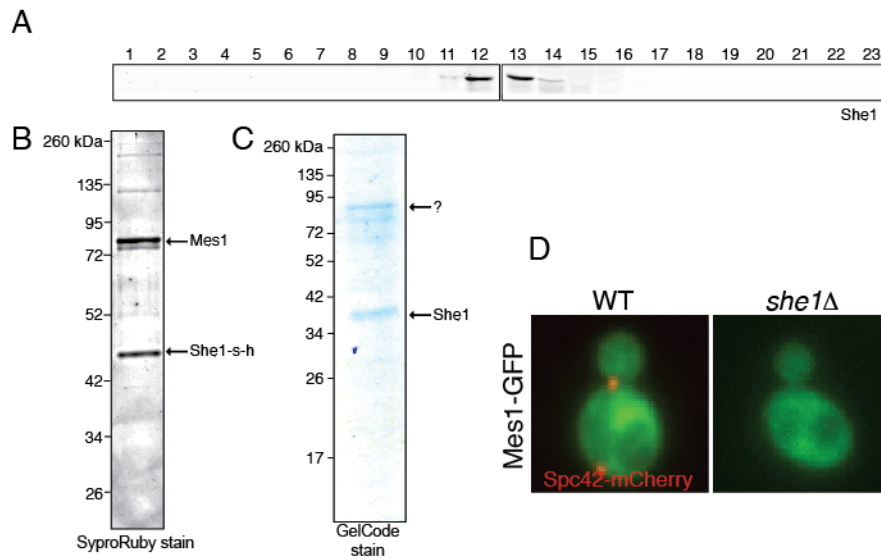
Figure 3.3: She1 interacts with Mes1 (A) A wild type yeast extract (DDY904) was prepared and subjected to size exclusion chromatography as described in materials and methods. Each of the lanes is an elution fraction **(B)** SDS-PAGE gel stained with SyproRuby showing purified She1-Strep-His from budding yeast (bottom band), and Mes1 (top band) as identified by mass spectrometry. **(C)** SDS-PAGE gel stained with GelCode showing purified She1 from budding yeast (bottom band), and a top band that is the same molecular size as Mes1 **(D)** Fluorescence image showing the localization of Mes1-GFP (green) in a wild type cell (left) and a *she1Δ* cell (right). Spc42-mCherry is shown in red only on the left cell.

3.3.4 She1 does not affect microtubule dynamics *in vitro*

To determine whether She1 alone is sufficient to destabilize or inhibit the growth of microtubules, we tested the effect of purified She1-HALO on microtubule dynamics in an *in vitro* TIRF assay (Gell et al., 2010). We used increasing amounts of She1-HALO and kept the concentration of free tubulin (Alexa 488-labeled tubulin) constant at 9 μM. As the concentration of She1-HALO increased, the growth rate of microtubules seemed to decrease (Figure 3.4 A, B). However, at the highest She1-HALO concentration (500 nM) the microtubule growth rate was similar to the one in the absence of She1-HALO. We also quantified the frequency of catastrophe events in the absence and in the presence of 250 nM She1-HALO. Analysis revealed that the presence of She1 does not significantly affect the frequency of catastrophes (Figure 3.4 C, D). We then tested whether She1 could interact with free tubulin dimers. If it did interact with free tubulin, She1 would be able to decrease the growth rate of microtubules by sequestering tubulin dimers and reducing the pool of free tubulin available for polymerization. To test for an interaction, we mixed equal molar amounts of purified She1-HALO with purified yeast tubulin and ran them in a gel filtration column (Figure 3.4 E). The UV elution peak of She1 + yeast tubulin was shifted towards a higher molecular weight complex, compared to the peaks of She-HALO or yeast tubulin alone. This suggests that indeed, She1-HALO can interact with yeast tubulin, forming a complex of higher molecular weight than any of the proteins alone.

She1-HALO didn't seem to have a very strong effect on microtubule dynamics. Since She1-HALO was purified from bacteria, it is not expected to have any biologically relevant posttranslational modifications. Woodruff and colleagues, (2010) showed that She1 activity is activated by Ipl1-mediated phosphorylation, as a She1 phosphomutant for predicted Ipl1 phosphorylation sites (She1$_{5A}$) exhibits delayed spindle disassembly relative to contraction of the cytokinetic ring. To test whether phosphorylated She1 has a stronger destabilizing effect on microtubules, we purified a phosphomimetic mutant of She1-HALO, where the five Ipl1 consensus sites present in She1 had been mutated to aspartates (She1$_{5D}$-HALO). However, quantification showed that She1$_{5D}$-HALO did not have a significant effect on the growth rate of microtubules (Figure 3.4 F). Bim1 is a +TIP protein that tracks the growing microtubule plus end on its own, and that recruits other proteins to the end. We thought that for She1 to destabilize the microtubule, it might need to be transported to the end by Bim1. To test this hypothesis we repeated the same quantification of microtubule growth rate in the presence of She1$_{5D}$-HALO together with Bim1. However, as in the previous experiments, the microtubule growth rate was not significantly affected by the presence of both proteins (Figure 3.4 G).
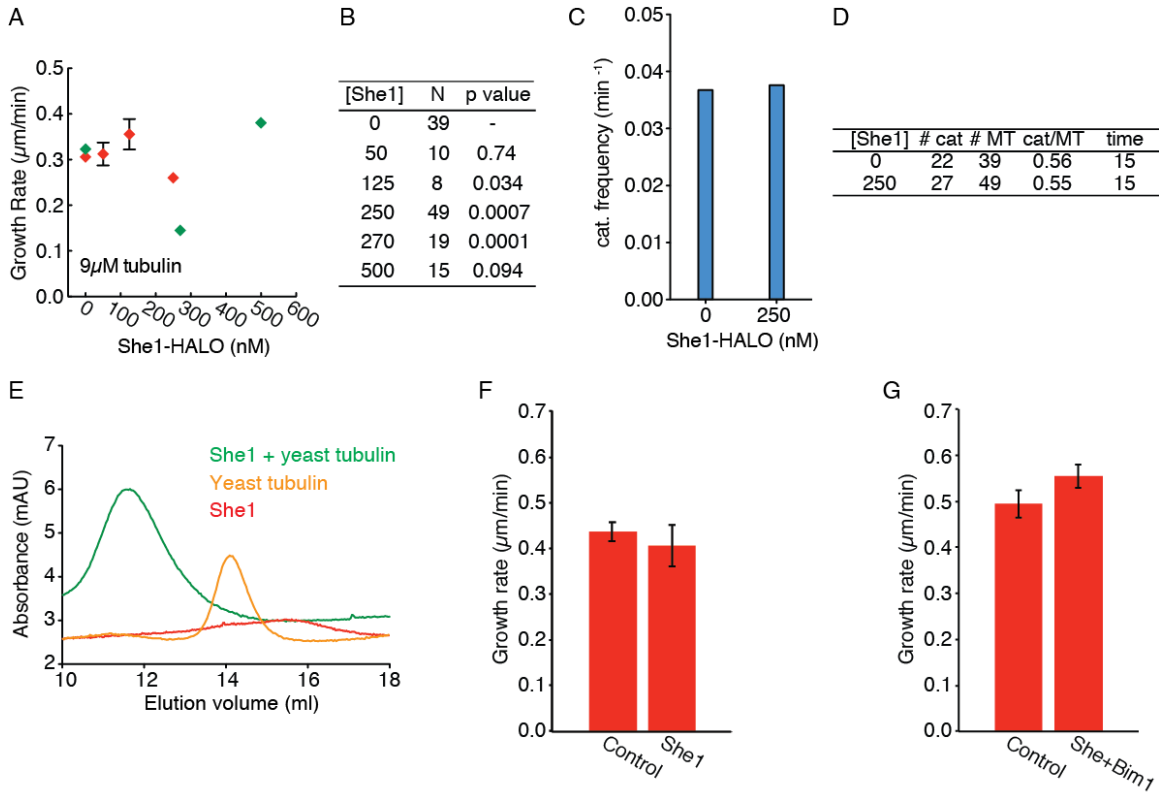
Figure 3.4: Effect of She1-HALO and She1_{5D}-HALO in microtubule dynamics (A) Microtubule growth rate (μm/min) plotted against the concentration of She1-HALO (nM), at a free tubulin concentration of 9μM. Data was collected on two separate days (each experimental day is represented as a different color, red or green). Error bars are SEM **(B)** Table showing the number of microtubules quantified for each concentration of She1-HALO plotted on "A", and the p-value for the growth rate at each concentration of She1-HALO compared to the microtubule growth rate without She1-HALO. **(C)** Catastrophe frequency (min^{-1}) plotted in the presence of 250 nM, or without She1-HALO **(D)** Table showing the number of catastrophe events observed, the number of microtubules quantified, the ratio of catastrophe events/number of microtubules, and the length of the movie (time, min) **(E)** UV absorbance profile of She1-HALO + yeast tubulin, yeast tubulin alone, or She1-HALO alone run through a size exclusion column as detailed in materials and methods **(F)** Microtubule growth rate (μm/min) quantified in the absence (control) or presence of 50 nM She1$_{5D}$-HALO. Error bars are SEM **(G)** Microtubule growth rate (μm/min) quantified in the absence (control) or presence of 50 nM She1$_{5D}$-HALO + 100 mM Bim1. Error bars are SEM.

3.3.5 Purification of untagged tubulin from budding yeast

As neither purified She1-HALO nor She1$_{5D}$-HALO had a robust effect on microtubule dynamics, we thought that the source of the tubulin might be important for She1's activity. She1 is a budding yeast protein, however, for the *in vitro* assays we were using tubulin from bovine brain to polymerize microtubules, as this has been the traditional way of studying the effect of microtubule-associated proteins on microtubule dynamics. However, recent studies have shown that using heterologous components to quantify the effect of a protein on microtubule dynamics can influence the result. For example Stu2, the budding yeast XMAP215, is a weak microtubule polymerase on porcine brain tubulin, however it can act as a strong microtubule polymerase using yeast tubulin: 500 nM of Stu2 can only increase the microtubule growth rate by 2-fold using porcine tubulin, however, a concentration of only 125 nM Stu2 increases the growth rate of budding yeast microtubules by 5-fold, demonstrating that the source of the tubulin does influence the effect that MAPs might have on the dynamics of microtubules (Podolski et al., 2014). Therefore, it seemed important to quantify the effect of She1 on microtubules polymerized from yeast tubulin.

Purification of untagged tubulin from a source other than porcine or bovine brain has proved to be challenging because tubulin is not abundant in most cell types, and the methods available tended to be long and tedious. Recently, however, a new method for purification of untagged tubulin from many sources, including budding yeast, was developed. This method relies on the TOG domain present in some MAPs like Stu2/XMAP215, that mediates their interaction with tubulin. The purification method is based on creating an affinity column with TOG domains, which would specifically bind to the tubulin present in the cell lysates. Since the nature of the interaction between the TOG domain and tubulin is electrostatic, pure tubulin can be easily eluted with a simple wash of the TOG column in high salt buffer (Widlund et al., 2012). We used that method to purify endogenous yeast tubulin from wild-type cells. In our hands the eluted tubulin from the TOG column had some contaminants. We therefore decided to add an additional purification step of size exclusion chromatography, which was able to separate the tubulin from the contaminants and yield highly pure yeast tubulin (Figure 3.5 A-D).

Purified yeast tubulin was used to test the interaction of She1-HALO with soluble tubulin dimers to investigate whether She1 acts as a tubulin-sequestering protein and slows down microtubule growth rate (Figure 3.4 E). Our preliminary results showed that She1 is able to interact with soluble yeast tubulin, suggesting that this could be the mechanism how it destabilizes microtubules. However, She1 did not affect microtubule dynamics in the *in vitro* TIRF assay (Figure 3.4 A-D) where bovine tubulin was used. These results strongly suggest that using yeast tubulin could be a relevant parameter to study She1 destabilizing activity on dynamic microtubules, and should be taken into consideration for future studies.
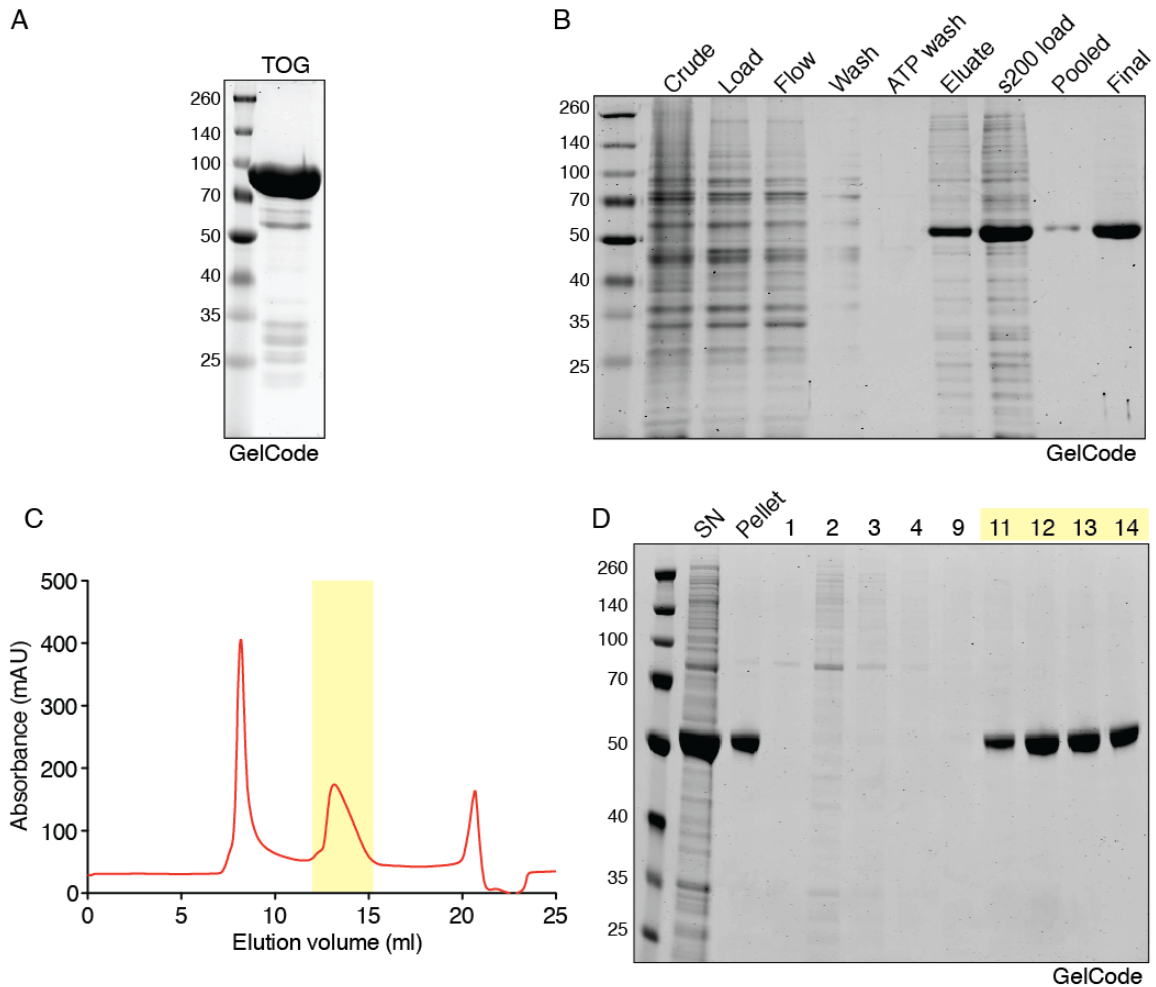
Figure 3.5: Purification of untagged tubulin from budding yeast (A) SDS-PAGE gel stained with GelCode showing purified TOG domain that was later bound to an NHS column, as described in materials and methods, to generate the affinity column to purify tubulin **(B)** Gel stained with GelCode showing the progress of the purification. Crude, dissolved yeast powder in lysis buffer; Load, cleared lysate loaded into TOG column; Flow, unbound fraction; Wash, wash of the TOG column; ATP wash, wash of TOG column with ATP; Eluate, pooled elution fractions from TOG column; s200 load, concentrated eluate injected into size exclusion column; Pooled, pooled fractions containing tubulin; Final, pooled fractions concentrated. At this step tubulin was aliquoted, flash frozen and stored at -80°C. **(C)** UV absorbance profile of tubulin eluting from the size exclusion column as a function of elution volume. The yellow region corresponds to the tubulin peak. **(D)** SDS-PAGE gel stained with GelCode. The gel shows supernatant (SN) and pellet (P) fractions of eluate from the TOG column, after being concentrated and subjected to ultracentrifugation. The SN was injected into the size exclusion column. 1-14 are elution fractions from gel filtration, and the yellow region represents the fractions containing tubulin that were pooled together, concentrated, aliquoted, flash frozen in liquid N_2 and stored at -80°C.

3.4 Discussion

Here, we have performed a biochemical characterization of She1, a microtubule-associated protein involved in spindle disassembly. The main goal for this project was to better understand the role of She1 during spindle disassembly, specifically test the hypothesis that She1 is a microtubule-destabilizing protein able to reduce or inhibit microtubule growth on its own. The approach that we took was to reconstitute microtubule dynamics in an *in vitro* TIRF assay, and quantify the effect of purified She1 on microtubule growth rate and catastrophe frequency. The first step, purification of She1, proved to be challenging. Previous studies have shown that She1 requires a tag such as GST or HALO to be soluble when purified from bacteria (Woodruff, 2011; Markus, et al 2012). We thought we could overcome the solubility problem by purifying She1 from budding yeast, since She1 would have all the posttranslational modifications that are present *in vivo*, and that might be required for its solubility. We also performed a screen to find the optimum buffer that would maximize She1 solubility. However, even when expressed in budding yeast cells, and having optimized the buffer composition, most of She1 was present in the pellet fraction when the crude lysate was subjected to high-speed centrifugation. A recent study from Markus and colleagues had had successful results using She1 with a HALO tag, and purified from bacteria. Since purification of soluble She1 from budding yeast seemed to be more challenging than expected, we decided to do the experiments using She1-HALO from bacteria. We demonstrated that She1-HALO is a microtubule-associated protein, and that its binding to microtubules is electrostatic, since it is disrupted by high salt. Our results are in agreement with previously published results, where they also found that She1 is indeed a MAP, and that its binding to microtubules is of electrostatic nature (Markus et al., 2012). However, their calculated affinity of She1 for microtubules is 0.8 µM, which contrasts with our value of 0.1 µM where we used the same cosedimentation assay. Our study therefore demonstrates, that She1 affinity for microtubules is higher than previously showed. In our hands, neither She1-HALO nor the active phosphomimetic mutant $She1_{5D}$-HALO significantly affected microtubule growth rate or catastrophe frequency. These results contrast with the results from Jeff Woodruff (Woodruff, 2011), where he showed that GST-She1 can inhibit the growth of microtubules from purified centrosomes. Jeff performed his experiment only once (personal communication), and therefore there is not enough data to be confident on this result. It is possible that his result was an artifact caused by the dimerization of She1 induced by the GST tag. A more reliable approach to confirm whether or not She1 alone destabilizes microtubules, would be to find the conditions that allow efficient purification of soluble She1 from budding yeast cells, and to test its effect on dynamic microtubules in the *in vitro* TIRF assay, using microtubules polymerized with budding yeast tubulin.

We also tested whether She1 can interact with soluble tubulin dimers, using size exclusion chromatography. The results suggested that She1 does interact with soluble yeast tubulin. However, the UV absorbance peaks were too shallow and therefore not reliable enough to have high confidence in the results. This experiment should be repeated with higher protein concentrations to get higher UV absorbance and more interpretable results. If She1 and soluble tubulin do interact, this would reduce the growth rate of microtubules. However, we did not observe any significant effect of She1-HALO on microtubule dynamics. This could be explained by the fact that we used tubulin from porcine brains in the *in vitro* TIRF assay, and budding yeast tubulin for the gel filtration experiment. These

results indicate that in the future, tubulin from budding yeast should be used to study She1's effects on microtubule dynamics.

We used two different affinity tags when we were optimizing the purification of She1 from budding yeast cells: a 7.5x myc tag and a 3x Streptavidin-9x His tag. In both cases we were able to purify small amounts of She1. Strikingly, in both purifications She1 co-purified at an equimolar ratio with a higher molecular weight protein, identified by mass spectrometry as Mes1. Microscopy analysis revealed that Mes1 is a cytosolic protein that does not colocalize with She1. Also, depletion of She1 did not change the localization of Mes1. It is possible, however that cytosolic She1 does interact with Mes1, and that Mes1 is involved in spindle positioning. Further studies of how depletion of Mes1 affects spindle orientation are needed to determine whether the interaction identified in this work is biologically relevant.

We hope that this work can help in the future to identify the specific mechanism of She1's effects during spindle disassembly, whether it directly destabilizes microtubules, or whether it does this through a downstream effector.

3.5 Materials and Methods

3.5.1 Plasmid construction

pIZ14 was generated from pIZ13 (generous gift from Damien D'amours lab, Université de Montréal), by digestion of the plasmid with BamHI and PacI followed by ligation with SHE1 ORF. pIZ14 takes advantage of an amplification loop driven by the pGAL1 promoter that allows the overexpression of big quantities of protein. For the overexpression loop to work it has to be expressed in IZ032, a yeast strain containing a PGAL1-GAL4 construct integrated in the LYS2 locus. Addition of galactose to the medium will induce high expression levels of GAL4 from the PGAL1-GAL4 construct. GAL4 is a transcription factor that activates the GAL1 promoter from pIZ14, generating an amplification loop that results in massive overexpression of the protein of interest, in this case, She1.

3.5.2 Protein purification

She1-HALO and She1$_{5D}$-HALO were purified as described on Markus et al., 2012 with some modifications. Proteins were expressed from pIZ20 and pIZ36 (generous gifts from Wei-Lih Lee, UMass) in BL21 Rosetta 2 cells (Novagen). Cells were induced with 0.1 mM IPTG for 16 hours at 16°C, harvested, washed and resuspended in 1x volume of 2x lysis buffer (60 mM HEPES pH 7.4, 100 mM potassium acetate, 4 mM magnesium acetate, 0.4 mM EGTA, 2 mM DTT, 0.8 mM PMSF, 1.4 mg/ml Pepstatin, 2x Complete Protease Inhibitor Cocktail (Roche)). Cells were lysed by sonication and the lysate was clarified by centrifugation at 50 Krpm for 20 min. The clarified lysate was adjusted to 0.2% Triton X-100 and incubated with GST-bind agarose (Novagen, previously washed with 1x lysis buffer) for 1 hour with rotation at 4°C. The resin was then washed 3 times with 10 volumes of wash buffer (30 mM HEPES pH 7.4, 50 mM potassium acetate, 2 mM magnesium acetate, 0.2 mM EGTA, 300 mM KCl, 0.1% Triton X- 100, 10% glycerol, 1 mM DTT, 0.4 mM PMSF, 0.7 mg/ml Pepstatin, 1x Complete Protease Inhibitor Cocktail (Roche)), and then 5 more times with TEV digest buffer (10 mM Tris pH 8.0, 150 mM KCl, 0.1% Triton X-100, 10% glycerol, 1 mM DTT). The resin was finally resuspended in TEV digest buffer supplemented with 0.017 mg/ml TEV protease and incubated for 2 hours at 16°C with rotation. The

resulting eluate was concentrated and injected into a size exclusion column (Superdex 200 10/300 GL, GE Healthcare) equilibrated in GF buffer (10 mM Tris pH 8.0, 500 mM KCl, 0.1% Triton X-100, 10% glycerol). Elution fractions were subjected to SDS-PAGE and silver stain. The fractions containing pure She1-HALO or She1$_{5D}$-HALO were pooled together, concentrated using an Amicon centrifugal filter unit (EMD Millipore), aliquoted, flash frozen in liquid N$_2$, and stored at -80°C. Bim1 was purified as described in section 3.5.1 of this dissertation.

For purification of She1-Strep-His, pIZ14 was transformed into IZ032. An overnight preculture was used to inoculate 2 liters of synthetic medium supplemented with 2% raffinose and dropout Uracil and Leucine and grown for 16 hours at 30°C. Cultures were induced with 2% galactose for 6 hours at 25°C, harvested by centrifugation, drop frozen and lysed using a 6870 Freezer/Mill (SPEX SamplePrep, Metuchen, NJ). 10 grams of yeast powder were thawed in 3.6 ml of 3x lysis buffer (150 mM Tris pH 8.0, 1.5 M KCl, 24% glycerol, 3 mM PMSF, 150 mM Arg/Glu, and 3x Complete Protease Inhibitor Cocktail without EDTA (Roche)), centrifuged for 20 min at 80,000 rpm in a Beckman TLA100.3 rotor (Beckman Coulter) at 4°C, and the clear supernatant was centrifuged again another 15 min at the same speed and temperature. Clarified lysate was injected into a HisTrap HP column (GE Healthcare), washed with Wash buffer (50 mM Tris pH 8.0, 0.5 M KCl, 8% glycerol, 1 mM PMSF, 50 mM Arg/Glu) and eluted using a gradient of Elution buffer (50 mM Tris pH 8.0, 0.5 M KCl, 8% glycerol, 1 mM PMSF, 50 mM Arg/Glu, 500 mM imidazole). Elution fractions containing She1 were pooled together, concentrated using an Amicon centrifugal filter unit (EMD Millipore), and incubated with Strep-Tactin beads (Qiagen) previously washed in wash buffer (50 mM Tris pH 8.0, 0.5 M KCl, 8% glycerol, 1 mM PMSF, 50 mM Arg/Glu) for 1 hour at 4°C. Beads were washed with wash buffer and She1-Strep-His was eluted with elution buffer (50 mM Tris pH 8.0, 0.5 M KCl, 8% glycerol, 1 mM PMSF, 50 mM Arg/Glu, 2.5 mM desthiobiotin). Elution fractions were concentrated, aliquoted, and flash frozen in liquid N$_2$.

Tubulin was purified from budding yeast as previously described (Widlund et al., 2012), with the following modifications. Elution fractions from the TOG column were concentrated using an Amicon centrifugal filter unit (EMD Millipore), and injected into a size exclusion column (Superdex 200 10/300 GL, GE Healthcare) equilibrated in GF buffer (80 mM Pipes pH 6.9, 1 mM EGTA, 1 mM MgCl$_2$, 100 μM GTP). Elution fractions were subjected to SDS-PAGE followed by staining with GelCode. Fractions containing tubulin were pooled together, concentrated to 20-25 μM, aliquoted and flash frozen in liquid N$_2$.

3.5.3 Microtubule cosedimentation assay

For the microtubule binding assay, purified She1-HALO was diluted in binding buffer (10 mM Tris pH 8.0, 50mM KCl, 0.1% Triton X-100, 10% Glycerol, 1mM DTT, 50 μM taxol) and combined with an equal volume of preassembled taxol-stabilized microtubules, resulting in 100 nM She1-HALO for all the conditions, and the final microtubule concentration indicated in each figure. The mixture was incubated for 20 min at room temperature, followed by centrifugation at 50 krpm at 25°C for 15 min. Supernatant and pellet fractions were collected, subjected to SDS-PAGE, transferred to a nitrocellulose membrane and blotted using anti-She1 and anti-Tub1 antibodies. To determine the K$_D$ the fraction of She1 bound to microtubules (fraction present in the pellet) was plotted against the concentration of microtubules and then fitted to the following equation using Prism:

$$\%bound = B_{max} \times \left(\frac{(K_d + [S] + [M]) - \sqrt{(K_d + [S] + [M])^2 - (4[S][M])}}{2[S]} \right) + b$$

where [S] equals the concentration of She1 (100 nM), [M] is the concentration of microtubules and b is the y-intercept.

3.5.4 Size exclusion chromatography

To investigate the oligomerization state of She1 *in vivo*, Yeast were grown to OD_{600} around 1.2 in YPD, pelleted and washed in cold water. The pellets were drop-frozen and pulverized using a 6870 Freezer/Mill (SPEX SamplePrep, Metuchen, NJ). For each gram of yeast powder, 1 ml of lysis buffer (100 mM HEPES pH 7.4, 300 mM NaCl, 2 mM EGTA, 2 mM DTT) and protease inhibitors (Protease Inhibitor Cocktail Set IV; Calbiochem, Merck4Biosciences, Billerica, CA) were added. Yeast powder was dissolved in lysis buffer by gently mixing on ice. The cell lysate was clarified by centrifugation at 350,000 x g for 20 min at 4°C. The cleared lysate (total protein concentration was ~20 mg/ml.) was collected, and 500 μl were injected into a Superose 6, 10/300 GL size exclusion column (GE Healthcare) previously equilibrated in buffer (50 mM HEPES pH 7.4, 150 mM NaCl, 1 mM EGTA, 1 mM DTT). Elution was performed at a flow rate of 0.4 ml/min and 0.75 ml aliquots were collected, subjected to SDS-PAGE and immunoblotting using an anti-She1 antibody.

To determine whether purified She1-HALO interacts with free tubulin dimers (purified from budding yeast), equimolar amounts of tubulin and She1-HALO (3 μM), yeast tubulin alone (3 μM), or only She1-HALO (3 μM) in a total volume of 50 μl (proteins were diluted in BRB80 to reach that final volume) were precleared by ultracentrifugation at 90 krpm for 5 min at 4°C and injected into a Superdex 200 10/300 GL column (GE Healthcare) pre-equilibrated in BRB80 buffer (80 mM Pipes pH 6.9, 1 mM EGTA, 1 mM $MgCl_2$) and run at a flow rate of 0.5 ml/min. The elution profile for each condition is plotted.

3.5.5 Live-cell imaging

For live-cell microscopy, cells were grown to log phase at 25°C in imaging media (synthetic medium lacking tryptophan and with 2% glucose) and immobilized on Concanavilin A-coated 25mm round #1.5 coverslips. Images were processed using ImageJ software.

Images were obtained using a Nikon Eclipse Ti microscope (Nikon Instruments, Melville, NY) controlled by MetaMorph (Molecular Devices, Sunnyvale, CA), and equipped with a Plan Apo VC 100x/1.4 Oil OFN25 DIC N2 objective, a MOV-2000 piezo stage (Applied Scientific Instrumentation, Eugene, OR), a Perfect Focus System (Nikon), a temperature-controlled enclosure (InVivo Scientific, St. Louis, MO), and a Neo sCMOS camera (Andor Technology Ltd., South Windsor, CT).

3.5.6 Dynamic microtubule assay

For the dynamic microtubule assay with Alexa Fluor 488-labeled tubulin, polymerized from GMPCPP-stabilized rhodamine-labeled microtubule seeds, TIRF microscopy was used as previously described (Gell et al., 2010). The imaging buffer

consisted of 80 mM PIPES pH 6.8, 1 mM $MgCl_2$, 1 mM EGTA, pH 6.8, 20 mM glucose, 20 μg/ml glucose oxidase, 8 μg/ml catalase, 0.1 mg/ml casein, and 1 mM GTP.

Table 3.1 Yeast strains used in this study

Strain name	Mating type	Genotype
DDY904	*MATα*	*leu2-3,112 lys-801 his3Δ200 ura3-52*
IZ066	*MATa*	*MES1-GFP::HIS SPC42-mCherry::KanMX leu2-3,112 lys-801 his3Δ200 ura3-52*
IZ068	*MATa*	*MES1-GFP::HIS ; she1Δ::LEU leu2-3,112 lys-801 his3Δ200 ura3-52*
IZ032	*MATa*	*lys2::Pgal1:GAL4::lys2 pep4::HIS3 bar1::hisG ade2 leu2 his3 trp1 ura3*

Table 3.2: Plasmids used in this study

Plasmid name	Genotype
pIZ13	PGAL1::SMC5 ORF::3xSTII::9xHIS::T_{BRN2}
pIZ14	PGAL1::SHE1 ORF::3xSTII::9xHIS::T_{BRN2}
pIZ69	pProEX-HTb-GST-TEV:SHE1-HALO
pIZ36	pProEX-HTb-GST-TEV:SHE1$_{5D}$-HALO

CHAPTER 4

The plus end-tracking protein complex Kip2-Bim1-Bik1 protects the growing microtubule against Kip3-induced catastrophe.

The work presented in this chapter is a collaboration with the laboratory of Jonathon Howard to continue a project that had been started in the 2014 Physiology course in Woods Hole. All the experiments presented here were done hand-by-hand by me and Anneke Hibbel, a graduate student from the Howard lab, during my 5-week stay in the Howard lab at the Max Planck Institute for Molecular Cell Biology and Genetics in Dresden, Germany.

4.1 Abstract

Microtubules switch stochastically between phases of polymerization (growth) and depolymerization (shrinkage), and in the cell this dynamicity has to be tightly regulated. However, how microtubule-associated proteins achieve this regulation is still poorly understood. Here, we report how the antagonistic kinesins Kip2 and Kip3 regulate microtubule length using purified proteins and total internal reflection fluorescence (TIRF) microscopy. In addition, as Kip2 is known to interact with +TIPs Bik1 and Bim1, both *in vivo* and *in vitro*, we probed how these +TIPs affect microtubule dynamics in combination with Kip2 and Kip3. We found that both Kip2 and Bim1 promote microtubule growth in a partly additive manner, whereas Bik1 did not affect microtubule dynamics. Surprisingly, both Kip2 and Bim1 protect the growing microtubule plus-end from the catastrophe inducing action of Kip3.

4.2 Introduction

The mitotic spindle is a dynamic structure formed by microtubules. Microtubules are polar filaments that are inherently dynamic; they alternate between periods of growth and sudden shrinkage events. The switching from slow growth to rapid shrinking is termed catastrophe, whereas the switching from shrinkage to growth is termed rescue (Walker et al., 1988). This process is termed dynamic instability (Mitchison and Kirschner., 1984). The four parameters of dynamic instability define a threshold between unlimited microtubule growth and steady-state dynamics (Verde et al., 1992). These steady-state dynamics per se lead to a broad distribution of microtubule lengths. In the cell, microtubule dynamics are tightly regulated, which results in a more narrow distribution of microtubule lengths (Howard and Hyman., 2007). This control of microtubule length requires a precise balance between the phases of slow growth and rapid shrinkage at the microtubule plus end. How this balance is achieved is still poorly understood.

Microtubule dynamics in the cell are regulated by microtubule-associated proteins (MAPs) (Howard and Hyman, 2007; Vaart et al., 2009). These MAPs can be categorized into three classes. The first class consists of proteins that increase microtubule growth rate, termed microtubule polymerases, such as XMAP215 (Gard and Kirschner., 1987; Brouhard et al., 2008) and Kip2 (Hibbel et al., 2015). The second class of MAPs that regulate microtubule dynamics are proteins that track the growing microtubule plus-ends, termed +TIPs, such as CLIP-170 (Perez et al., 1999) and EB1 (Mimori-Kiyosue et al., 2000) (reviewed in Akhmanova and Steinmetz., 2010). The third class of MAPs consists of proteins that disassemble microtubules, termed microtubule depolymerases, which can remove the stabilizing GTP-cap (Kinoshita et al., 2006), triggering microtubule catastrophe. In short, MAPs can influence microtubule growth positively and negatively. Among the MAPs that regulate microtubule dynamics are molecular motors of the kinesin superfamily, such as the budding yeast kinesins Kip3 and Kip2. Kip3 is a length-dependent microtubule

catastrophe factor (Varga et al., 2006). By contrast, Kip2 promotes microtubule growth as a length-dependent microtubule polymerase and anti-catastrophe factor (Hibbel et al., 2015). Interestingly, these antagonistic kinesins are found on the same set of microtubules in the yeast cell.

Here, we studied how the antagonistic kinesins Kip2 and Kip3 regulate microtubule length using purified proteins and total internal reflection fluorescence (TIRF) microscopy. In addition, as Kip2 is known to interact with +TIPs Bik1 and Bim1, both *in vivo* (Carvalho et al., 2004; Caudron et al., 2008) and *in vitro* (Roberts et al., 2014; Blake-Hodek et al., 2010). We probed how these +TIPs affect microtubule dynamics in combination with Kip2 and Kip3. We found that both Kip2 and Bim1 promote microtubule growth in a partly additive manner, whereas Bik1 did not affect microtubule dynamics. Surprisingly, both Kip2 and Bim1 protect the growing microtubule plus-end from the catastrophe inducing action of Kip3.

4.3 Results

4.3.1 The plus end tracking complex Kip2-Bim1-Bik1 increases average microtubule length

To investigate the effect of the Kip2-Bim1-Bik1 complex on microtubule length *in vitro*, we reconstituted this protein complex on dynamic microtubules using purified components in an *in vitro* TIRF assay (Gell et al., 2010, Figure 4.1A). Dynamic microtubules were grown with 12 µM porcine tubulin and (combinations of) 40 nM Kip2, 22 nM Bik1-eGFP and 200 nM Bim1-eGFP, in the presence of 1 mM ATP. We chose to work at 40 nM Kip2, because at this concentration the effect on growth rate and catastrophe frequency is saturated (Hibbel et al., 2015). The concentrations of Bik1-eGFP and Bim1-eGFP reflect the relative physiological concentrations of the proteins in the cell with respect to Kip2, based on Ghaemmaghami et al., 2003. Microtubule lengths of freshly polymerized (green) microtubules were measured ten minutes after addition of Kip2, Bim1-eGFP and/or Bik1-eGFP and free tubulin to the surface-bound microtubule seeds (Figure 4.1 B). As expected, Kip2 increased the average microtubule length from 1.3 ± 0.16 µm to 7.0 ± 0.33 µm ($n = 48$ and 32 respectively, $p < .0001$ (Welch's unpaired t- test)). Bim1-eGFP also increased microtubule length to 8.8 ± 0.64 µm ($n = 29$, $p < .0001$ (Welch's unpaired t-test)). By contrast, Bik1-eGFP decreased the average microtubule length to 0.70 ± 0.14 µm ($n = 33$, $p < .01$ (Welch's unpaired t-test)).

Next, the effect on microtubule length of combinations of Kip2, Bim1-eGFP and Bik1-eGFP was probed. The combination of Bim1-eGFP and Kip2 further increased average microtubule length to 11.0 ± 0.37 µm ($n = 20$, $p < .0001$ (Welch's unpaired t-test)). By contrast, the combination of Bik1-eGFP and Kip2 did not affect microtubule length compared to Kip2 alone (7.0 ± 0.33 µm compared to 7.6 ± 0.47 µm ($n = 32$ and 21 respectively, $p = .35$ (Welch's unpaired t -test)). The combination of Bim1-eGFP and Bik1-eGFP did also not affect microtubule length compared to Bim1 alone (8.8 ± 0.64 µm compared to 7.9 ± 0.53 µm, $n = 29$ and 25 respectively, $p = .29$ (Welch's unpaired t-test)). Finally, the complete plus end tracking protein complex Kip2-Bim1-eGFP-Bik1-eGFP affected microtubule length to the same extent as the combination of Kip2 with Bim1-eGFP (11.0 ± 0.37 µm compared to 10.2 ± 0.44 µm, $n = 20$ in both conditions, $p = .21$ (Welch's unpaired t-test)). Thus, whereas both Kip2 and Bim1 alone are sufficient to increase

microtubule length, Bik1 is neither necessary nor sufficient to increase microtubule length *in vitro*. This contrasts what was suggested by genetic studies in Carvalho et al., 2004. In summary, the plus end tracking protein complex Kip2-Bim1-Bik1 increases microtubule length *in vitro*, through partially additive effects of Kip2 and Bim1.

4.3.2 The plus end tracking complex Kip2-Bim1-Bik1 increases microtubule growth rate

To quantify whether Bik1 and Bim1 influence microtubule dynamics, kymographs were created from the time-lapse images of the dynamic microtubule assay (Figure 4.1 C, D). These kymographs revealed that microtubules were dynamic both with and without Bik1-eGFP and Bim1-eGFP present in the assay. To characterize the effect of Bik1-eGFP and Bim1-eGFP on microtubule dynamics, the microtubule growth rate was analyzed in the presence of (combinations of) these proteins. As expected, we found that Kip2 alone increased the microtubule growth rate from 0.34 ± 0.01 μm/min to 0.76 ± 0.04 μm/min ($n = 116$ and 30 respectively, $p < .0001$ (Welch's unpaired t-test)). Bim1-eGFP also increased the microtubule growth rate, to 0.85 ± 0.04 μm/min ($n = 37$, $p < .0001$ (Welch's unpaired t-test)). By contrast, Bik1-eGFP lowered the microtubule growth rate, to 0.30 ± 0.01 μm/min ($n = 78$, $p < .001$, Welch's unpaired t-test). Thus, in contrast to the indications from genetic studies, Bik1 does not possess microtubule polymerase activity. The measured stimulating effect of Bim1 on microtubule growth rate and the growth rate decreasing effect of Bik1 are in agreement with previous studies from Blake-Hodek et al., 2010.

To reconstitute the combinatorial effects of the plus end tracking protein complex Kip2-Bim1-Bik1, the dynamic microtubule assay was performed in the presence of Kip2 plus Bim1-eGFP, Kip2 plus Bik1-eGFP, Bim1-eGFP plus Bik1-eGFP and finally Kip2, Bim1-eGFP and Bik1-eGFP (Fig, 3.1 E). These experiments revealed that the combination of Kip2 and Bim1-eGFP increased microtubule growth rate in a partially additive manner, from 0.76 ± 0.04 μm/min at 40 nM Kip2 to 1.15 ± 0.03 μm/min when both proteins were present in the assay ($n = 30$ and 26 respectively, $p < .0001$ (Welch's unpaired t-test)). By contrast, addition of Bik1-eGFP to Kip2 did not affect microtubule growth rate compared to the growth rate in the presence of only Kip2 (0.80 ± 0.47 μm/min and 0.76 ± 0.04 μm/min respectively, $n = 16$ and 30 respectively, $p = .45$ (Welch's unpaired t-test)). The addition of Bik1-eGFP to Bim1-eGFP did also not affect the growth rate compared to the growth rate in the presence of only Bim1-eGFP (0.86 ± 0.04 μm/min and 0.85 ± 0.04 μm/min respectively, $n = 33$ and 37 respectively, $p = .89$ (Welch's unpaired t-test)). Finally, the combination of Kip2, Bim1-eGFP and Bik1-eGFP increased the microtubule growth rate to the same extent as the combination of Kip2 and Bim1-eGFP (1.07 ± 0.03 μm/min and 1.15 ± 0.03 μm/min respectively, $n = 25$ and 26 respectively, $p = .06$ (Welch's unpaired t-test)). In summary, Kip2 and Bim1 both increase microtubule growth rates. Their partially additive effects suggest that they do so via different mechanisms. Bik1 seems to have a subtle effect decreasing microtubule growth rate, but in combination with either Kip2 or Bim1, its effect is lost.

4.3.3. The plus end tracking complex Kip2-Bim1-Bik1 prevents microtubule catastrophe

Next, we investigated the effect of the three proteins on microtubule catastrophe

frequency (Fig. 3.1 F). To quantify catastrophe frequency, the total number of catastrophes observed per experimental condition was divided by the total duration of microtubule growth of all microtubules in that experimental condition (K_{cat}). In agreement with previous findings (Hibbel et al., 2015), Kip2 decreased K_{cat} from 0.14 ± 0.02 per minute to < 0.004 per minute (mean ± SE, n = 90 and 0 respectively, p < .0001 (Welch's unpaired t-test)). Bim1-eGFP also decreased K_{cat}, albeit to a lesser extent, to 0.03 ± 0.01 per minute (n = 10, p < .0001 (Welch's unpaired t-test)). Bik1-eGFP did not affect K_{cat} (0.14 ± 0.02 per minute, n = 60, p = .84 (Welch's unpaired t-test)).

Kip2 in combination with either Bim1-eGFP or Bik1-eGFP decreased K_{cat} to the same extent as Kip2 alone (0.004 ± 0.004 catastrophe events per minute in both conditions, n = 0 in both conditions, p = .05 (Welch's unpaired t-test)). The addition of Bik1-eGFP to Bim1-eGFP did not affect K_{cat} compared to Bim1-eGFP alone (0.04 ± 0.01 catastrophe events per minute, n = 18, p = .18 (Welch's unpaired t-test)). Finally, Kip2, Bim1-eGFP and Bik1-eGFP in combination decreased K_{cat} to the same extent as Kip2 alone (< 0.001 catastrophe events per minute, n = 0, p = .96 (Welch's unpaired t-test)), but significantly more than Bim1-eGFP alone (p < .05 (Welch's unpaired t-test)). Thus, Kip2 alone and in complex with Bim1 or Bik1 completely suppresses microtubule catastrophe. Bim1 also prevents catastrophe, but to a lesser extent than Kip2 does. Bik1 does not affect K_{cat}, neither alone nor in complex. In summary, the plus end tracking protein complex Kip2-Bim1-Bik1 prevents microtubule catastrophe. Taken together, these results show that the Kip2-Bim1-Bik1 complex promotes microtubule growth, and that this effect is mediated by partially additive activity of Kip2 and Bim1.

Figure 4.1: Combinatorial regulation of microtubule dynamics by Kip2, Bim1-eGFP and Bik1-eGFP. (A) Schematic of the experimental design. Alexa-488-labeled porcine tubulin (green) in solution polymerizes onto the ends of GMPCPP-stabilized, rhodamine-labeled microtubules (red) bound to the coverslip with anti-rhodamine antibodies (blue), in the presence or absence of Kip2, Bim1-eGFP and/or Bik1-eGFP. The surface of the flow chamber is imaged using TIRF microscopy, which minimizes background from the fluorescent tubulin in solution. **(B)** Representative kymographs of microtubules grown with 12 μM porcine tubulin (left), tubulin plus 40nM Kip2, tubulin plus 200 nM Bim1-eGFP, or tubulin plus 22 nM Bik1-eGFP (from left to right), in the presence of 1 mM ATP. Scale bar = 2 μm. **(C, D)** Representative kymographs of microtubules grown with 12 μM porcine tubulin and combinations of 40 nM Kip2, 200 nM Bim1-eGFP and/or 22 nM Bik1-eGFP, in the presence of 1 mM ATP. Scale bar = 2 μm. **(E)** Bar chart showing microtubule length (mean ± SE) at t = 10 minutes after the start of the experiment of microtubules grown with 12 μM porcine tubulin in 1 mM ATP for control and (combinations of) 40 nM Kip2, 200 nM Bim1-eGFP and 22 nM Bik1-eGFP. **(F)** Microtubule growth rate (mean ± SE) of microtubules grown with 12 μM porcine tubulin in 1 mM ATP for control and (combinations of) 40 nM Kip2, 200 nM Bim1-eGFP and 22 nM Bik1- eGFP. **(G)** Catastrophe frequency (mean ± SE) of microtubules grown with 12 μM porcine tubulin in 1 mM ATP for control and (combinations of) 40 nM Kip2, 200 nM Bim1 and 22 nM Bik1.

4.3.4 Kip2 and Bim1 protect the growing microtubule against the destabilizing activity of Kip3

Previously, it was suggested that during spindle positioning astral microtubules remain protected against Kip3-mediated catastrophe until they reach the bud cortex (Fukuda *et al.*, 2014). We wondered whether the Kip2-Bim1-Bik1 complex, which is present on astral microtubules, could protect the microtubule against the destabilizing effect of Kip3. To test this hypothesis, we quantified the effect on microtubule growth rate and catastrophe frequency of Kip3 together with the single components and the whole Kip2-Bim1-Bik1 complex (Figure 4.2 A-D). The concentrations of Kip3, Bim1 and Bik1 reflect their relative physiological concentrations in the cell with respect to Kip2, based on Ghaemmaghami et al., 2003. In agreement with previous reports (Gardner et al., 2011), Kip3 alone reduced the growth rate of dynamic microtubules 1.5 fold, from 0.34 ± 0.01 μm/min to 0.23 ± 0.02 μm/min ($n = 23$, $p < .0001$). By contrast, the combination of Kip3 with either Kip2 or Bim1 increased microtubule growth rate to 0.79 ± 0.06 μm/min and 0.98 ± 0.03 μm/min respectively ($n = 24$ and 47, $p < .0001$). The combination of Kip3 with the whole complex also increased microtubule growth rate to the same extent as the complex without Kip3, to 1.0 ± 0.03 μm/min ($n = 31$, $p = 0.31$). Thus, whereas Kip3 alone decreases the growth rate of microtubules, this effect is lost in the presence of either Kip2 or Bim1.

Kip3 is a microtubule catastrophe factor (Gardner et al., 2011). In agreement, in our hands Kip3 increased K_{cat} by 2.6 fold from 0.14 ± 0.01 min^{-1} ($n = 90$) to 0.36 ± 0.08 min^{-1} ($n = 20$, $p < .05$). Interestingly, the combination of Bim1 with Kip3 reduced K_{cat} by 7-fold compared with Kip3 alone $(0.05 \pm 0.01$ min^{-1}, $n = 23$, $p < .005)$ and by almost 3 fold compared to control ($p < 0.0001$). Strikingly, no catastrophe events were ever observed when Kip3 was combined with Kip2 ($K_{cat} = 0.001$, $n = 0$, $p < .0001$). Similarly, the Kip2-Bim1-Bik1 complex was also able to protect the microtubule against Kip3, and as for Kip2 alone, we do not observe any catastrophe event ($K_{cat} = 0.001$, $n = 0$, $p < 0.0001$). These results suggest that the stabilizing effect of both Bim1 and Kip2 dominates over the destabilizing activity of Kip3. Thus, the Kip2-Bim1-Bik1 complex protects the growing microtubule against the depolymerizing activity of Kip3.
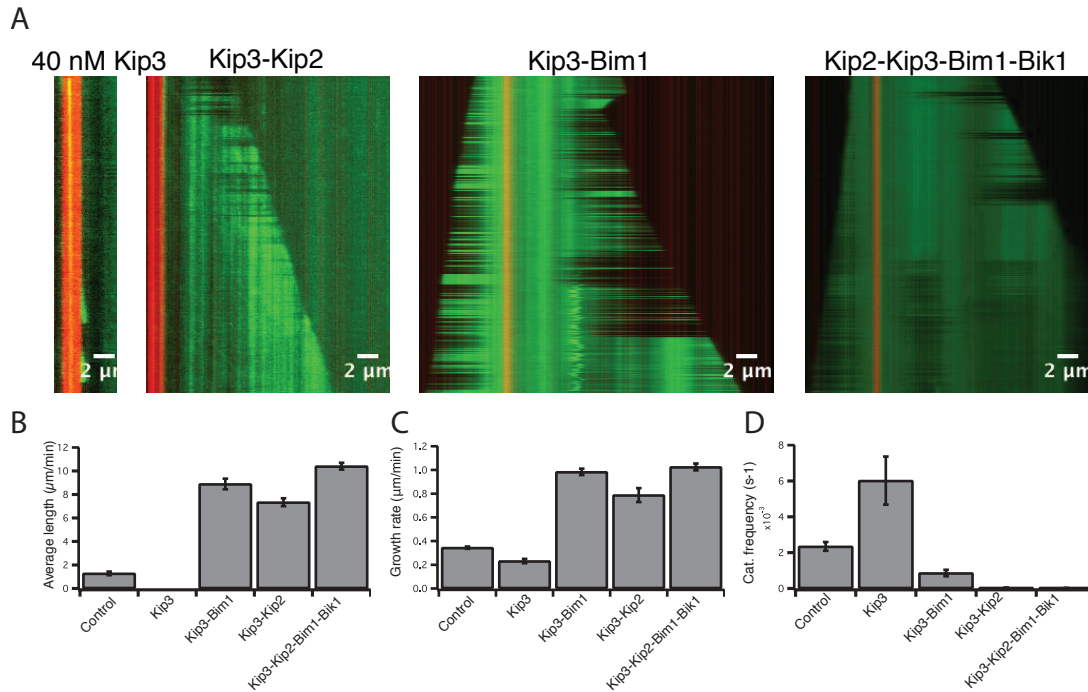
Figure 4.2: Kip2 and Bim1 protect the growing microtubule against Kip3. (A) Representative kymographs of microtubules grown with 12 µM porcine tubulin plus 40 nM Kip3 (left), tubulin plus 40 nM Kip3 and 40 nM Kip2, tubulin plus 40 nM Kip3 and 200 nM Bim1-eGFP, and tubulin plus 40 nM Kip3, 40 nM Kip2, 200 nM Bim1 and 22 nM Bik1-eGFP (from left to right), in the presence of 1 mM ATP. Scale bar = 2 µm. **(B)** Bar chart showing microtubule length (mean ± SE) at t = 10 minutes after the start of the experiment of microtubules grown with 12 µM porcine tubulin in 1 mM ATP for control and (combinations of) 40 nM Kip3, 40 nM Kip2, 200 nM Bim1-eGFP and 22 nM Bik1-eGFP. **(C)** Microtubule growth rate (mean ± SE) of microtubules grown with 12 µM porcine tubulin in 1 mM ATP for control and (combinations of) 40 nM Kip3, 40 nM Kip2, 200 nM Bim1-eGFP and 22 nM Bik1-eGFP. **(D)** Catastrophe frequency (mean ± SE) of microtubules grown with 12 µM porcine tubulin in 1 mM ATP for control and (combinations of) 40 nM Kip3, 40 nM Kip2, 200 nM Bim1-eGFP and 22 nM Bik1-eGFP.

4.3.5 Kip3 has a low affinity for the growing microtubule, and it leaves the microtubule upon arrival at the plus end

The antagonistic kinesins Kip2 and Kip3 use the same microtubule track *in vivo* (reference). To better understand the mechanism by which the growth-promoting activity of Kip2 dominates over the destabilizing effect of Kip3, we purified both kinesins with a fluorescent tag (Kip2-taqRFP and Kip3-eGFP) and observed their behavior on microtubules. In agreement with previous observations, we found that Kip3-eGFP has high affinity for GMPCPP-stabilized microtubules and at 40nM Kip3-eGFP it decorates the whole lattice. However, at the same Kip3-eGFP concentration but in the presence of soluble tubulin dimers that polymerize at the ends of the GMPCPP seeds, we were only able to see Kip3-

eGFP on microtubules at a single molecule level, suggesting that Kip3 has higher affinity for free tubulin than for the growing microtubule (Figure 4.3 A, B). When we combined equimolar concentrations of Kip3-eGFP and Kip2-taqRFP (40nM), we still observed single molecules of Kip3-eGFP localizing on the microtubule, whereas Kip2-taqRFP decorated the whole growing microtubule (Figure 4.4), indicating that Kip2 has higher affinity than Kip3 for dynamic microtubules.

We next quantified the end-residence time of Kip3 at the plus end before it dissociates from the microtubule. We argued that for Kip2 to be able to protect the microtubule and minimize the access of Kip3 to the end, it should remain at the plus-end for longer time than Kip3. Hibbel and colleagues (2015) show that Kip2 remains and tracks the growing plus-end for up to 10 seconds before it dissociates from the microtubule. Interestingly, Kip3 does not track the plus end, instead, it leaves the microtubule upon reaching the plus end (Figure 4.3 C).
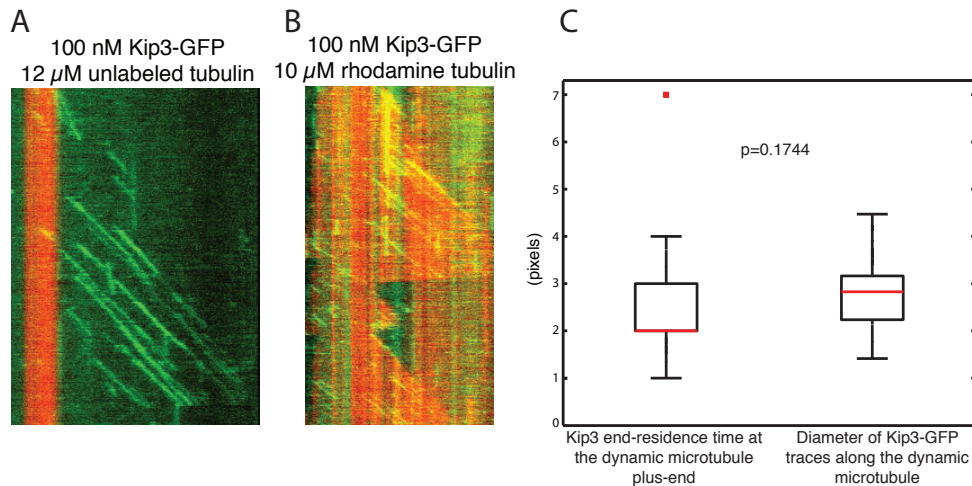

Figure 4.3: The affinity of Kip3 for dynamic microtubules is low and the motor dissociates from the growing plus end. (A) Representative kymograph of a microtubule grown with 12 μM unlabeled porcine tubulin plus 100 nM Kip3-GFP in the presence of 1mM ATP. Microtubule was grown out of a GMPCPP-stabilized microtubule seed (red). **(B)** Representative kymograph of a microtubule grown with 10 μM rhodamine-labeled porcine tubulin plus 100 nM Kip3-GFP in the presence of 1mM ATP. **(C)** Box chart comparing the width in pixels of the Kip3-GFP traces when they reach the growing microtubule plus end, with the width of the Kip3-GFP traces along the dynamic microtubule. The difference in width of the traces is not statistically significant, suggesting that Kip3 leaves the microtubule upon arrival at the microtubule plus end.

4.3.6 Kip2 out-competes Kip3 at the microtubule plus end

The fact that Kip2 has higher affinity for the growing microtubule and that it has a longer end-residence time, gives Kip2 an advantage over Kip3 to dominate microtubule dynamics. To further understand the mechanism how Kip2 protects the plus end against Kip3 we addressed two different scenarios. One possibility is that Kip2 promotes microtubule growth at a rate faster than Kip3 velocity. That way, Kip3 can never reach the

growing microtubule plus end and destabilize it. In that situation the different end-residence time of Kip2 and Kip3 would not be a relevant parameter. Another possible way would be that Kip3 can reach the end, however Kip2 is already there and prevents Kip3 from inducing a catastrophe. To distinguish between these two possibilities we measured Kip3 velocity and microtubule growth rate at different tubulin concentrations (6μM and 12μM) and constant Kip2 concentration (Figure 4.4 A-D). We found that Kip3 velocity is independent of the tubulin concentration and, that it is fast enough to reach the growing microtubule plus end. Our findings support the latter scenario, and suggest that even though Kip3 is able to reach the growing plus end, the presence of Kip2 likely prevents Kip3 from accessing its site of action, and thus protects the plus end from undergoing catastrophe.
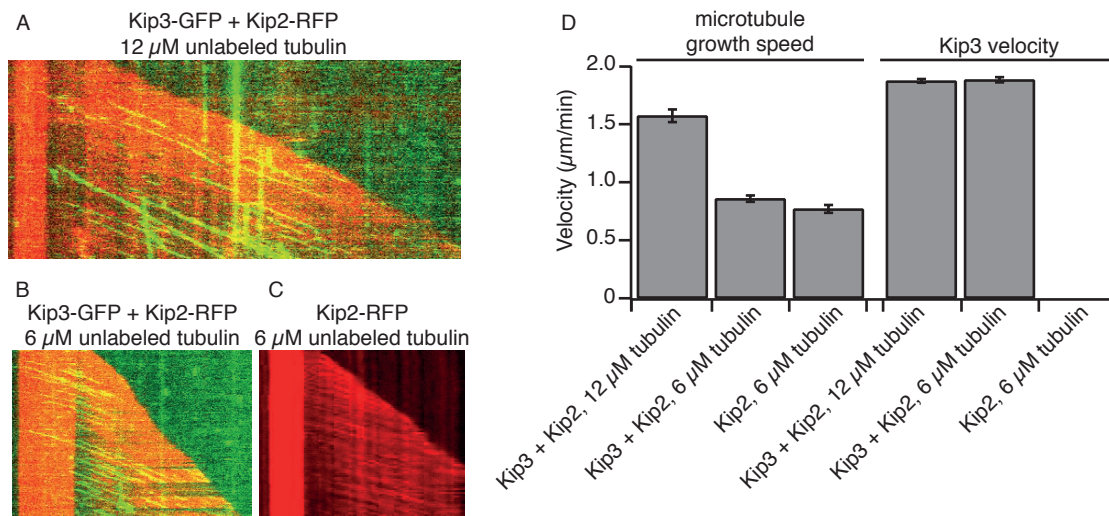
Figure 4.4: Kip2 out-competes Kip3 at the microtubule plus end. (A) Representative kymograph of a microtubule grown with 12 μM unlabeled porcine tubulin plus 40 nM Kip2 and 40nM Kip3, in the presence of 1 mM ATP. At equimolar concentrations Kip2 decorates the entire growing microtubule, while only single molecules of Kip3 are visible. A 488 nm laser in TIRF was used to be able to visualize Kip3, however Kip2 bound to the growing microtubule was visible with regular epifluorescence. **(B)** Representative kymograph of a microtubule grown with 6 μM unlabeled porcine tubulin plus 40 nM Kip2 and 40nM Kip3, in the presence of 1 mM ATP. **(C)** Representative kymograph of a microtubule grown with 6 μM unlabeled porcine tubulin plus 40 nM Kip2 in the presence of 1 mM ATP. **(D)** Bar chart (mean ± SE) comparing microtubule growth speed versus Kip3 velocity (μm/min) in three different conditions: 40 nM Kip3 and 40 nM Kip2 plus 12 μM tubulin; 40 nM Kip3 and 40 nM Kip2 plus 6 μM tubulin; and 40 nM Kip2 plus 6 μM tubulin.

4.4 Discussion

The budding yeast protein complex formed by Kip2, Bim1 and Bik1 is present on astral microtubules, where it is important for targeting dynein to the microtubule plus end and for positioning the spindle. Here we have shown that the ternary protein complex promotes microtubule growth and prevents catastrophes *in vitro*. Our results indicate that Kip2 and Bim1 are the main contributors to that effect. We have also shown that, as a complex, Kip2 and Bim1 together increase the growth rate of dynamic microtubules in an additive way. Bik1 does not seem to play an important role in the regulation of microtubule dynamics, neither alone nor in the complex. Our results for Kip2, Bim1 and Bik1 alone agree with previous studies (Blake-Hodek *et al.,* 2010; Hibbel *et al.*, 2015) where they used similar protein concentrations.

Fukuda and colleagues (2014) have shown that during spindle positioning, cytoplasmic microtubules that grow into the bud are protected against Kip3-induced catastrophe, which allows effective positioning of the spindle perpendicular to the division plane. We found that the ternary complex protects microtubules against Kip3. Our results show that the growth promoting effect of the complex is able to dominate over the destabilizing activity of Kip3, as catastrophe events are completely eliminated. To get a better understanding of the mechanism how the complex protects the microtubule we focused on investigating the interplay between Kip2 and Kip3. We chose Kip2 because it has an antagonistic effect with Kip3 *in vivo* and because they both use the same microtubule track. Moreover, Kip2 seems to be the main contributor from the complex in preventing Kip3 from inducing catastrophes. We first looked at Kip3-GFP on GMPCPP-stabilized microtubules. It completely decorated the whole lattice and, as expected, microtubules quickly shrank from their plus-end. However, when we repeated the assay using the same concentration of Kip3-GFP (40 nM) but with soluble tubulin to create dynamic microtubules, we only saw single Kip3-GFP molecules walking towards the plus end. This suggests that Kip3-GFP has higher affinity for soluble tubulin than for the microtubule itself, and that it might also act as a tubulin-sequestering protein. In the same line, Su and colleagues (2011) showed by using gel filtration that the C-terminal tail of Kip3 strongly binds tubulin dimers. We also quantified that at a concentration of 40 nM Kip3-GFP, where we observed single molecules walking towards the plus-end of dynamic microtubules, the catastrophe frequency was increased by 2.6 fold, which agrees with previous studies (Gardner *et al.,* 2011). This observation supports the idea that not many molecules of Kip3 need to reach the end to induce a catastrophe. We then looked at the behavior of fluorescent Kip2 on dynamic microtubules. Strikingly, the same concentration of Kip2-RFP (40 nM) on unlabeled dynamic microtubules decorated the whole lattice. The affinity of Kip2 for the microtubule was so high that we were able to clearly see the unlabeled growing microtubule through its interaction with Kip2-RFP by simple epifluorecence microscopy. Our data shows that Kip2 has a higher affinity than Kip3 for dynamic microtubules and provides a way in which Kip2 activity can dominate over Kip3. We also observed that Kip3 molecules leave the microtubule upon reaching its plus-end. This contrasts with the long end-residence time of Kip2, which has been measured to be around 10 seconds (Hibbel *et al.,* 2014). Having a longer end-residence time gives Kip2 advantage over Kip3. A longer end-residence time together with the fact that Kip2 has also higher affinity for the growing microtubule makes sure that there will always be a molecule of Kip2 at the plus end.

Up to this point we could think of two different mechanisms for how Kip2 could protect the microtubule against Kip3. One possibility is that Kip2 promotes microtubule growth at a rate faster than Kip3 velocity. In this scenario, Kip3 would never be able to reach the plus-end and destabilize it. An alternative possibility is that even though Kip3 reaches the microtubule end, Kip2 sterically hinders Kip3 access to the site it needs to bind to destabilize the microtubule. Our results have shown that Kip3 is actually fast enough to reach the microtubule but that once there it cannot induce a catastrophe event. These results indicate that the presence of Kip2 at the microtubule end prevents Kip3 from gaining access to the binding site it needs to induce a catastrophe event. Kip2 could also protect the microtubule against Kip3 by an allosteric mechanism: Kip3 might be able to reach its action site where it would normally induce curvature of the terminal tubulin dimer and hence promote a catastrophe. However, Kip2 binding to a different site might promote a straight conformation of the terminal tubulin dimers that Kip3 cannot overcome.

In order to efficiently regulate the changes in microtubule dynamics required to orchestrate the different stages of mitosis, a complex network of proteins is needed. An example is the regulation of spindle length, which is determined by the relative activity of the two antagonistic motors Cin8/Kip1 and Kar3. It has been suggested that the changes in the balance of those two forces triggers the onset of spindle elongation (Saunders et al., 1997). More recent work has shown how two plus end-binding proteins, EB1 and XMAP215, act synergistically to strongly promote microtubule growth (Zanic et al., 2012). The work shown in this dissertation proposes a molecular mechanism for how the two antagonistic kinesins Kip2 and Kip3 coordinate their activities to position the mitotic spindle, and furthers our understanding of how a complex network of MAPs can act collectively to modulate microtubule dynamics and successfully complete mitosis.

4.5 Materials and methods

4.5.1 Protein purification

Full length 6xHis-Kip2 and 6xHis-Kip2-RFP were expressed in SF+ cells using baculovirus expression. The lysis buffer consisted of 50 mM NaH_2PO_4 pH 8.0, 300 mM NaCl, 0.1% Tween-20, 2 mM Mg-ATP, 10 mM imidazole, and protease inhibitors. The lysate was intected into a HisTrap column (GE Healthcare), washed with wash buffer (50 mM NaH_2PO_4 pH 8.0, 300 mM NaCl, 2 mM Mg-ATP, and 100 mM imidazole), and eluted withelution buffer (50 mM NaH_2PO_4 pH 8.0, 300 mM NaCl, 2 mM Mg-ATP, and 300 mM imidazole). To cleave the 6xHis tag, the protein was incubated with PreScission protease (GE Healthcare) overnight at 4°C. The next day, Kip2 and Kip2-RFP were injected into a Sephadex 200 column pre-equilibrated with protein storage buffer (80 mM PIPES pH 6.8, 1 mM $MgCl_2$, 1 mM EGTA, 10% glycerol, 1 mM Mg-ATP, and 1 mM DTT. Final protein concentration was measured by Bradford and the purified protein were aliquoted, snap-frozen in liquid nitrogen and stored at -80°C. Purification of full length Kip3 and Kip3-GFP was performed as previously described (Varga et al., 2006).

Full-length 6xHis-Bik1-eGFP was expressed in SF+ cells using baculovirus expression and purified using affinity chromatography over His-affinity columns, as described in (Blake-Hodek et al., 2010). Affinity column purification success was checked by SDS-PAGE and Western blot using anti-6xHis as a primary antibody. Next, 6xHis-tags were enzymatically cleaved from the protein using PreScission protease. Finally, Bik1-eGFP was

purified to homogeneity by gel filtration over a Sephadex 200 column, which was pre-washed with protein storage buffer. Protein stability was confirmed by SDS-PAGE and enzymatic cleavage of the 6xHis-tag from the protein of interest by Western blot using anti-6xHis-antibody.

Purification of Bim1-eGFP was kindly performed by Dr. Aliona Bogdanova. Full-length 6xHis-Bim1-eGFP was expressed in *E.coli* and purified using affinity chromatography over His-affinity columns, as described in (Blake-Hodek et al., 2010). Affinity column purification success was checked by SDS-PAGE and Western blot using anti-6xHis as a primary antibody. Next, 6xHis-tags were enzymatically cleaved from the protein using PreScission protease. Finally, Bim1-eGFP was purified to homogeneity by gel filtration over a Sephadex 200 column, which was pre-washed with protein storage buffer. Protein stability was confirmed by SDS-PAGE and enzymatic cleavage of the 6xHis-tag from the protein of interest by Western blot using anti-6xHis-antibody.

4.5.2 Microscopy assay and imaging conditions

For the dynamic microtubule assay with Alexa Fluor 488-labeled tubulin, or unlabeled tubulin polymerized from GMPCPP-stabilized rhodamine-labeled microtubule seeds, TIRF microscopy was used as previously described (Gell et al., 2010). The imaging buffer consisted of 20 mM PIPES pH 6.8, 1 mM $MgCl_2$, 1 mM EGTA, pH 6.8, 100 mM KCl, 20 mM glucose, 20 µg/ml glucose oxidase, 8 µg/ml catalase, 0.1 mg/ml casein, 1 mM DTT, 0.001% tween-20, 1 mM GTP and 1 mM Mg-ATP.

Imaging was performed with an Andor iXon camera on a Zeiss (Oberkochen, Germany) Axiovert 200M microscope with a Zeiss 100x/1.46 plan apochromat oil objective and standard filter sets. An objective heater (Zeiss) was used to warm the sample to 28°C. All experiments were performed at least three times on three different days. To quantify the dynamic parameters of microtubules kymographs of at least 30 microtubule growth events were created and analyzed using ImageJ. To quantify the growth rate, the slope of the kymographs was measured using Microsoft Excel, and to quantify the catastrophe frequency, the total number of events was divided by the total observation time.

CHAPTER 5
Perspectives and future directions

The goal of my dissertation research was to better understand how mitosis is regulated. I focused on investigating the processes of spindle disassembly (Chapters 2 and 3), and spindle positioning (Chapter 4), as they have been much less studied compared to spindle assembly or chromosome segregation. The work presented in this dissertation has expanded our understanding of how these two processes function. However, there are still many questions that remain to be answered. In this final Chapter I am presenting topics to follow up on that would extend the findings described here and further our understanding of spindle function.

5.1 Proposed directions for future studies of spindle disassembly

5.1.1 Phosphoregulation of the interaction between the CPC and Kip1

According to the model proposed in Chapter 2, there is a signaling event during late anaphase that triggers an interaction between the CPC and Kip1. This signaling event restricts the midzone recruitment of the CPC to the end of late anaphase. A phosphorylation site mutant of Sli15 lacking Ipl1 sites (CPC[17A]) concentrates to the midzone prematurely (Nakajima et al., 2011), suggesting that dephorphorylation of Sli15 by Glc7 might be that signaling event. It would be very interesting to test whether CPC(17A) has a higher affinity for Kip1 than CPC(WT). This possibility can be readily tested using a pull-down assay, or by repeating the bulk microscopy assay shown in Figure 2.8, and comparing the fluorescence intensity of CPC(WT)-GFP + Kip1 vs CPC(17A)-GFP + Kip1 on microtubules.

Ipl1 is phosphorylated by Cdk1. This phosphorylation prevents the CPC from binding Bim1 before anaphase. During anaphase, Cdc14-mediated dephosphorylation of Cdk1 sites on Ipl1 allows the CPC to interact with and phosphorylate Bim1 at the midzone to promote spindle disassembly (Zimniak et al., 2012; Woodruff et al., 2010). It is important to also investigate whether Cdk1/Cdc14 phosphorylation/dephosphorylation of Ipl1 affects the interaction between the CPC and Kip1.

5.1.2 Role of Kip3 in CPC recruitment to the midzone

The cell biology data described on Chapter 2 demonstrates that both Kip1 and Kip3 are required for CPC midzone localization. However, the biochemistry experiments show that purified Kip1 alone is able to transport the CPC to the microtubule end. Therefore, the exact role of Kip3 in this process is still unknown. There are at least three possible ways how Kip3 could function: a) by directly transporting the CPC to the MT end just like Kip1 does, b) by making the transport of CPC by Kip1 more efficient, or 3) by facilitating the attachment of CPC to the midzone. It would be really interesting to test each of this possibilities to identify the exact role of Kip3 in this process.

5.1.3 Study of cell cycle regulation of CPC function *ex vivo*

Our laboratory has recently developed a cell-free assay that uses budding yeast whole cell lysates to study the contribution of specific microtubule-binding proteins to cell cycle-dependent microtubule dynamics, maintaining a similar cellular context to the one *in vivo*. This assay is similar to the one used on Chapter 4 where microtubule seeds are attached to the coverglass, however, instead of Alexa488-labeled tubulin, it uses cell extracts of strains

expressing GFP-labeled tubulin that polymerizes off the seeds and allows quantification of microtubule dynamics in different mutant strains.

By using this novel assay it would be possible to observe the movement of CPC on microtubules by simply incubating Nbl1-GFP-expressing whole cell extracts with long rhodamine microtubules attached to the coverglass. Anti-GFP antibodies attached to quantum dots would make the Nbl1-GFP signal brighter and more photostable. Once the assay is optimized, it would be interesting to generate cdc mutants to arrest the Nbl1-GFP strain at different stages of the cell cycle and determine how CPC movement on microtubules is cell-cycle regulated. By looking at whole cell extracts of *NBL1-GFP kip1Δ kip3Δ* strains it would also be possible to study the dependence of CPC movement on Kip1 and Kip3.

5.1.4 Identify the mechanism by which She1 destabilizes spindle microtubules

Woodruff and colleagues showed that She1 is a microtubule-destabilizing factor involved in spindle disassembly. Chapter 3 of this dissertation describes the biochemical approaches that I took to test whether She1 alone is sufficient to destabilize or inhibit microtubule growth. My results showed that neither purified She1-HALO nor a constitutively active purified phosphomimetic She1$_{5D}$-HALO affects microtubule dynamics. These results suggest that the destabilizing effect of She1 on microtubules is indirect. However I think that the hypothesis that She1 is a microtubule-destabilizing factor on its own cannot be completely ruled out yet. It is possible that the HALO tag alters the function of She1, and it is also possible that there are other posttranslational modifications required to activate She1's microtubule-destabilizing activity. Therefore, it might be worthwhile to develop the optimum conditions that allow purification of She1 from budding yeast without affects its posttranslational modifications, and conditions that also allow removal of the tag while maintaining She1 solubility. I have screened manyf different conditions to increase She1 solubility, including different buffers, pH, salt concentrations, induction time and temperature among others (see Chapter 3) that can be used in future studies. Also, tubulin from budding yeast should be used instead of porcine brain tubulin.

If using an untagged version of She1 purified from budding yeast still confirms that She1 does not have a destabilizing effect on microtubules, it would be interesting to investigate the indirect mechanism. Jeff Woodruff performed an analysis of She1 interacting partners by mass spectrometry (Woodruff, 2011). One of those proteins could be the downstream effector of She1. To test this possibility, candidate proteins would have to be purified and their effects on microtubule dynamics tested in an *in vitro* reconstitution assay like the one used for She1 in Chapter 3, or for Kip2/Bim1/Bik1/Kip3 in Chapter 4.

5.2 Proposed directions for future study of spindle positioning

5.2.1 Test the effect of combined Kip2 and Kip3 on yeast microtubules

Chapter 4 is a biochemical investigation of how the antagonistic activities of Kip2 and Kip3 are coordinated to achieve proper spindle positioning. This chapter also examines the contribution of the MAPs Bim1 and Bik1 to this process. All the microtubule-binding proteins used in the study are budding yeast proteins. However, porcine brain tubulin was

used to polymerize microtubules. The reason for this shortcut was that the effect of each of the individual proteins on microtubule dynamics was the same regardless of whether yeast or mammalian tubulin was used. However, it is possible that when combining the above-mentioned proteins the source of the tubulin used influences their collective behavior. Therefore, it is important to test the effect of combined Kip2/Bim1/Bik1 and also Kip2/Bim1/Bik1/Kip3 on dynamic yeast microtubules.

References

Akhmanova, A., and Steinmetz, MO. 2010. Microtubule +TIPs at a glance. *J Cell Sci.* 123(Pt 20):3415-9.

Blake-Hodek, KA., Cassimeris, L., and Huffaker, T.C. 2010. Regulation of microtubule dynamics by Bim1 and Bik1, the budding yeast members of the EB1 and CLIP-170 families of plus-end tracking proteins. Mol Biol Cell. 21(12):2013-23.

Brouhard, G.J., Stear, J.H., Noetzel, T.L., Al-Bassam, J., Kinoshita, K., Harrison, S.C., Howard, J., and Hyman, A.A. 2008. XMAP215 is a processive microtubule polymerase. *Cell.* 132(1):79-88.

Buvelot, S., Tatsutani, S.Y., Vermaak, D., and Biggins, S. 2003. The budding yeast Ipl1/Aurora protein kinase regulates mitotic spindle disassembly. *J Cell Biol.* 1 60(3):329-39.

Carmena, M., Wheelock, M., Funabiki, H., and Earnshaw, W.C. 2012. The chromosomal passenger complex (CPC): from easy rider to the godfather of mitosis. *Nat Rev Mol Cell Biol.* 13(12):789-803.

Carminati, J.L., and Stearns, T. 1997. Microtubules orient the mitotic spindle in yeast through dynein-dependent interactions with the cell cortex. *J Cell Biol.* 138(3):629-41.

Carvalho, P., Gupta, M.L Jr., Hoyt, M.A., and Pellman, D. 2004. Cell cycle control of kinesin-mediated transport of Bik1 (CLIP-170) regulates microtubule stability and dynein activation. *Dev Cell.* 6(6):815-29.

Caudron, F., Andrieux, A., Job, D., and Boscheron, C. 2008. A new role for kinesin-directed transport of Bik1p (CLIP-170) in Saccharomyces cerevisiae. *J Cell Sci.* 121(Pt 9):1506-13.

Cheeseman, I.M., Anderson, S, Jwa, M., Green, E.M., Kang, J., Yates III, J.R., Chan, C.S., Drubin, D.G., and Barnes, G. 2002. Phospho-regulation of kinetochore-microtubule attachments by the Aurora kinase Ipl1p. *Cell.* 111:163–172.

Cooke, C.A., Heck, M.M., and Earnshaw, W.C. 1987 The inner centromere protein (INCENP) antigens: movement from inner centromere to midbody during mitosis. *J Cell Biol.* 105(5):2053-67.

Cormier, A., D.G. Drubin., and G. Barnes. 2013. Phosphorylation regulates kinase and microtubule binding activities of the budding yeast chromosomal passenger complex in vitro. *J. Biol. Chem.* 288(32):23203-11.

Cui, H., Ghosh, S.K., and Jayaram, M. 2009. The selfish yeast plasmid uses the nuclear motor Kip1p but not Cin8p for its localization and equal segregation. *J Cell Biol.* 185(2):251-64.

Ferenz, N.P., Gable, A., and Wadworth, P. 2010. Mitotic functions of kinesin-5. Semin *Cell Dev Biol.* 21(3):255-9.

Fridman, V., Gerson-Gurwitz, A., Shapira, O., Movshovich, N., Lakämper. S., Schmidt, C.F., and Gheber, L. 2013. Kinesin-5 Kip1 is a bi-directional motor that stabilizes microtubules and tracks their plus-ends in vivo. *J Cell Sci.* 126(Pt 18):4147-59.

Fukuda, Y., Luchniak, A., Murphy, E.R., and Gupta, M.L Jr. 2014. Spatial control of microtubule length and lifetime by opposing stabilizing and destabilizing functions of Kinesin-8. *Curr Biol.* 24(16):1826-35.

Gard, D.L., and Kirschner, M.W. 1987. Microtubule assembly in cytoplasmic extracts of Xenopus oocytes and eggs. *J Cell Biol.* 105(5):2191-201.

Gardner, M.K., Zanic, M., Gell, C., Bormuth, V., and Howard, J. 2011. Depolymerizing kinesins Kip3 and MCAK shape cellular microtubule architecture by differential control of catastrophe. *Cell.* 147(5):1092-103.

Gell, C., Bormuth, V., Brouhard, G.J., Cohen, D.N., Diez, S., Friel, C.T., Helenius, J., Nitzsche, B., Petzold, H., Ribbe, J., Schäffer, E., Stear, J.H., Trushko, A., Varga, V., Widlund, P.O., Zanic, M., and Howard, J. 2010. Microtubule dynamics reconstituted in vitro and imaged by single-molecule fluorescence microscopy. *Methods Cell Biol.* 95:221-45.

Ghaemmaghami, S., Huh, W.K., Bower, K., Howson, R.W., Belle, A., Dephoure, N., O'Shea, E.K., and Weissman, J.S. 2003. Global analysis of protein expression in yeast. *Nature.* 425(6959):737-41.

Gruneberg, U., Neef, R., Honda, R., Nigg, E.A., and Barr, F.A. 2004. Relocation of Aurora B from centromeres to the central spindle at the metaphase to anaphase transition requires MKlp2. *J. Cell Biol.* 166:167–172.

Hibbel, A., Bogdanova, A., Mahamdeh, M., Jannasch, A., Storch, M., Schäffer, E., Liakopoulos, D., and Howard, J. 2015. Kinesin Kip2 enhances microtubule growth in vitro through length-dependent feedback on polymerization and catastrophe. *eLife.* 4:e10542.

Hildebrandt, E.R., and Hoyt, M.A. 2000. Mitotic motors in *Saccharomyces cerevisiae. Biochim Biophys Acta.* 1496(1):99-116.

Howard, J., and Hyman, A.A. 2007. Microtubule polymerases and depolymerases. *Curr Opin Cell Biol.* 19(1):31-5.

Hoyt, M.A., He, L., Loo, K,K,, and Saunders, W.S. 1992. Two Saccharomyces cerevisiae kinesin-related gene products required for mitotic spindle assembly. *J Cell Biol.* 118(1):109-20.

Hoyt, M.A., He, L., Totis, L., and Saunders, W.S. 1993. Loss of function of Saccharomyces cerevisiae kinesin-related CIN8 and KIP1 is suppressed byKAR3 motor domain mutations. *Genetics.* 135(1):35-44.

Hsu, J.Y., Sun, Z.W., Li, X., Reuben, M., Tatchell, K., Bishop, D.K., Grushcow, J.M., Brame, C.J., Caldwell, J.A., Hunt, D.F., Lin, R., Smith, M.M., and Allis, C.D. 2000. Mitotic phosphorylation of histone H3 is governed by Ipl1/aurora kinase and Glc7/PP1 phosphatase in budding yeast and nematodes. *Cell.* 102:279–291.

Huang, B., and Huffaker, T.C. 2006. Dynamic microtubules are essential for efficient chromosome capture and biorientation in *S. cerevisiae. J Cell Biol.* 175:17–23.

Khmelinskii, A., and Schiebel, E. 2008. Assembling the spindle midzone in the right place at the right time. *Cell cycle.* 7(3):283-6.

Kitagawa, M., Fung, S.Y., Onishi, N., Saya, H., Lee, S.H. 2013. Targeting Aurora B to the equatorial cortex by MKlp2 is required for cytokinesis. *PLoS One.* 8(6):e64826.

Kotwaliwale, C.V., Frei, S.B., Stern, B.M, and Biggins, S. 2007. A pathway containing the Ipl1/aurora protein kinase and the spindle midzone protein Ase1regulates yeast spindle assembly. *Dev Cell.* 13(3):433-45.

Longtine, M.S., McKenzie. A 3rd., D.J. Demarini., N.G. Shah., A. Wach., A. Brachat., P. Philippsen., J.R. Pringle. 1998. Additional modules for versatile and economical PCR-based gene deletion and modification in *Saccharomyces cerevisiae. Yeast.* 14(10):953-61.

Maddox, P.S., Bloom, K.S., and Salmon, E.D. 2000. The polarity and dynamics of microtubule assembly in the budding yeast *Saccharomyces cerevisiae.* Nat Cell Biol. 2(1):36-41.

Markus SM, Kalutkiewicz KA, Lee WL. 2012. She1-mediated inhibition of dynein motility along astral microtubules promotes polarized spindle movements. *Curr Biol.* 22(23):2221-30.

McNally, F.J. 2013. Mechanisms of spindle positioning. *J Cell Biol.* 200(2):131-140.

Mimori-Kiyosue, Y., Shiina, N., and Tsukita, S. 2000. The dynamic behavior of the APC-binding protein EB1 on the distal ends of microtubules. *Curr Biol.* 10(14):865-8.

Mitchison, T., and Kirschner, M. 1984. Dynamic instability of microtubule growth. *Nature.* 312(5991):237-42.

Molk., J.N, Salmon, E.D., and Bloom, K. 2006. Nuclear congression is driven by cytoplasmic microtubule plus end interactions in S. cerevisiae. *J Cell Biol.* 172(1):27-39.

Morawska, M., and Ulrich. H. 2013. An expanded tool kit for the auxin-inducible degron system in budding yeast. *Yeast.* 30(9):341-51.

Murata-Hori, M., Tatsuka, M., and Wang, Y.L. 2001. Probing the dynamics and functions of Aurora B kinase in living cells during mitosis and cytokinesis. *Mol Biol Cell.* 13(4):1099-108.

Nakajima, Y., Cormier, A, Tyers, R.G, Pigula, A., Peng, Y., Drubin, D.G., and Barnes, G. 2011. Ipl1/Aurora-dependent phosphorylation of Sli15/INCENP regulates CPC-spindle interaction to ensure proper microtubule dynamics. *J Cell Biol.* 194(1):137-53.

Norden, C., Mendoza, M., Dobbelaere, J., Kotwaliwale, C.V., Biggins, S., and Barral, Y. 2006. The NoCut pathway links completion of cytokinesis to spindle midzone function to prevent chromosome breakage. *Cell.* 125(1):85-98.

Pearson, C.G., and Bloom, K. 2004. Dynamic microtubules lead the way to spindle positioning. *Nat Rev Mol Cell Biol.* 5(6):481-92.

Perez, F., Diamantopoulos, G.S., Stalder, R., and Kreis, T.E. 1999. CLIP-170 highlights growing microtubule ends in vivo. *Cell.* 96(4):517-27.

Petersen, J., Paris, J., Willer, M., Philippe, M., and Hagan, I.M. 2001. The S. pombe aurora-related kinase Ark1 associates with mitotic structures in a stage dependent manner and is required for chromosome segregation. *J Cell Sci.* 114(Pt 24):4371-84.

Pinsky, B.A., Kung, C., Shokat, K.M., and Biggins, S. 2006b. The Ipl1-Aurora protein kinase activates the spindle checkpoint by creating unattached kinetochores. *Nat. Cell Biol.* 8:78–83.

Podolski, M., Mahamdeh, M., and Howard, J. 2014. Stu2, the budding yeast XMAP215/Dis1 homolog, promotes assembly of yeast microtubules by increasing growth rate and decreasing catastrophe frequency. *J Biol Chem.* 289(41):28087-93.

Roberts, A.J., Goodman, B.S., and Reck-Peterson, S.L. 2014. Reconstitution of dynein transport to the microtubule plus end by kinesin. *Elife.* 3:e02641.

Saunders, W.S., and Hoyt, M.A. 1992. Kinesin-related proteins required for structural integrity of the mitotic spindle. *Cell.* 70(3):451-8.

Saunders, W.S., Lengyel, V., and Hoyt, M.A. 1997. Mitotic spindle function in Saccharomyces cerevisiae requires a balance between different types of kinesin-related motors. *Mol Biol Cell.* 8(6):1025-33.

Shannon, K.B., and Salmon, E.D. 2002. Chromosome dynamics: new light on aurora B kinase function. *Curr Biol.* 12(13):R458-60.

Siller, K.H., and Doe, C.C. 2009. Spindle orientation during asymmetric cell division. *Nat Cell Biol.* 11(4):365-74.

Sproul, L.R., Anderson, D.J., Mackey, A.T., Saunders, W.S., and Gilbert, S.P. 2005. Cik1 targets the minus-end kinesin depolymerase kar3 to microtubule plus ends. *Curr Biol.* 15(15):1420-7.

Sun, Y., Leong, N.T., Wong, T., and Drubin, D.G. 2015. A Pan1/End3/Sla1 complex links Arp2/3-mediated actin assembly to sites of clathrin-mediated endocytosis. *Mol Biol Cell.* 26(21):3841-56.

van der Vaart, B., Akhmanova, A., and Straube, A. 2009. Regulation of microtubule dynamic instability. *Biochem Soc Trans.* 37(Pt 5):1007-13.

Varga, V., Helenius, J., Tanaka, K., Hyman, A.A., Tanaka, T.U., and Howard, J. 2006. Yeast kinesin-8 depolymerizes microtubules in a length-dependent manner. *Nat Cell Biol.* 8(9):957-62.

Verde, F., Dogterom, M., Stelzer, E., Karsenti, E., and Leibler, S. 1992. Control of microtubule dynamics and length by cyclin a- and cyclin b- dependent kinases in Xenopus egg extracts. *J Cell Biol.* 118(5):1097-108.

Wargacki, M,M,, Tay, J.C., Muller, E.G., Asbury, C.L., and Davis, T.N. 2010. Kip3, the yeast kinesin-8, is required for clustering of kinetochores at metaphase. *Cell cycle.* 9(13):2581-8.

Walczak, C.E., and Heald, R. 2008. Mechanisms of mitotic spindle assembly and function. *Int Rev Cytol.* 265:111-58.

Walker, R.A., O'Brien, E.T., Pryer, N.K., Soboeiro, M.F., Voter, W.A., Erickson, H.P., and Salmon, E.D. 1988. Dynamic instability of individual microtubules analyzed by video light microscopy: rate constants and transition frequencies. *J Cell Biol.* 107(4):1437-48.

Weaver, B.A., and Cleveland, D.W. 2006. Does aneuploidy cause cancer? *Curr Opin Cell Biol.* 19(2):246.

Widlund, P.O., Podolski, M., Reber, S., Alper, J., Storch, M., Hyman, A.A., Howard, J., and Drechsel, D.N. 2012. One-step purification of assembly-competent tubulin from diverse eukaryotic sources. *Mol Cell Biol.* 23(22):4393-401.

Winey, M., and O'Toole, E.T. 2001. The spindle cycle in budding yeast. *Nat Cell Biol.* 3(1):E23-7.

Winey, M., and Bloom, K. 2012. Mitotic spindle form and function. *Genetics.* 190(4):1197-224.

Woodruff, J.B., Drubin, D.G., and Barnes, G. 2009. Dynein-driven mitotic spindle positioning restricted to anaphase by She1p inhibition of dynactin recruitment. *Mol Biol Cell.* 20(13):3003-11.

Woodruff, J.B., Drubin, D.G., and Barnes, G. 2010. Mitotic spindle disassembly occurs via distinct subprocesses driven by the anaphase-promoting complex, Aurora B kinase, and kinesin-8. *J Cell Biol.* 191(4):795-808.

Woodruff, J.B. 2011. Mechanisms of mitotic spindle disassembly and positioning in *Saccharomyces cerevisiae* (Doctoral dissertation). Retrieved from eScholarship.

Woodruff, J.B., Drubin, D.G, and Barnes, G. 2012. Spindle assembly requires complete disassembly of spindle remnants from the previous cell cycle. *Mol Biol Cell.* 23(2):258-67.

Zanic, M., Widlund, P.O., Hyman, A.A., and Howard, J. 2012. Synergy between XMAP215 and EB1 increases microtubule growth rates to physiological levels. *Nat Cell Biol.* 15(6):688-93.

Zimniak, T., Stengl, K., Mechtler, K., and Westermann, S. 2009. Phosphoregulation of the budding yeast EB1 homologue Bim1p by Aurora/Ipl1p. *J Cell Biol.* 186(3):379-91.

Zimniak, T., Fitz, V., Zhou, H., Lampert, F., Opravil, S., Mechtler, K., Stolt-Bergner, P., and Westermann, S. 2012. Spatiotemporal regulation of Ipl1/Aurora activity by direct Cdk1 phosphorylation. *Curr Biol.* 22(9):787-93.